VORTEX BURSTING OVER A UNIT AREA ASPECT RATIO DELTA WING USING VORTEX PANELING METHODS

THESIS

Donald A. Lorey, Captain, USAF

AFIT/GAE/ENY/90D-14

DEPARTMENT OF THE AIR FORCE
AIR UNIVERSITY
AIR FORCE INSTITUTE OF TECHNOLOGY

Wright-Patterson Air Force Base, Ohio

AFIT/GAE/ENY/90D-14

VORTEX BURSTING OVER A UNIT AREA ASPECT RATIO DELTA WING USING VORTEX PANELING METHODS

THESIS

Donald A. Lorey, Captain, USAF

AFIT/GAE/ENY/90D-14

AFIT/GAE/ENY/90D-14

VORTEX BURSTING OVER A UNIT AREA ASPECT RATIO DELTA WING USING VORTEX PANELING METHODS

THESIS

Presented to the Faculty of the School of Engineering

of the Air Force Institute of Technology

Air University

In Partial Fulfillment of the

Requirements for the Degree of

Master of Science in Aeronautical Engineering

Donald A. Lorey, B.S.

Captain, USAF

December 1990

Approved for public release; distribution unlimited

Preface

The purpose of this effort was to determine if vortex paneling methods can compute the vortex bursting that occurs over a unit aspect ratio delta wing at high angles of attack. The leading-edge vortex flows dominate the flow field over such wings. The vortex breakdown, or bursting that occurs over the wing affects the lift and drag, as well as the moment-balance of the aircraft. It is therefore desirable to compute such effects if possible.

Multiple calculations were performed on both the ELXSI at the Air Force Institute of Technology, and the Cray-YMP at Ohio State University. The unreliability of the ELXSI provided great anxiety as to whether or not this thesis would be completed. However, the Cray-YMP worked quite well and was an invaluable, albeit limited, resource.

I would like to take this time to give appreciation to others. I would like to thank my thesis advisor Major Curt Mracek for his invaluable time, support, and assistance. I would also like to thank the other committee members, Captain Phil Beran, and Lieutenant Colonel DeJongh for their valuable inputs. I would also like to give thanks to all my classmates for their help and friendship. Finally, and most importantly, I would like to give thanks to my wife, Lora, for her support and understanding throughout the past one

and a half years.

Special thanks and remembrance is given to a fellow student and friend, Captain Wayne Wilsdon who died in an automobile accident during his tour at AFIT. His generosity and help made it possible for all to pass the Aerodynamics of Wings and Bodies course. His help, and friendship will not be forgotten.

Table of Contents

List of Figures

List of Tables

Abstract

A unit aspect ratio delta wing is analyzed to determine if a unsteady vortex panel method can calculate the vortex bursting of the vortex developed along the leading-edge. A two-dimensional vortex panel method is used to investigate wake splitting schemes of the vortex cores that comprise the vortex sheet, or wake. The worthier of the splitting methods is later implemented into the three-dimensional wake. The weighting values of the Kutta equations are investigated for the leading-edges, and are determined to be problem specific. An alternative approach to the management of the wake data is presented and implemented. The delta wing is then analyzed for 20.5 and 30 degrees angle of attack. The panel method produced a perturbation and enlargement in the wake at the two-thirds chord position over the wing at 30 degrees angle of attack, indicative of vortex breakdown. However, a qualitative comparison with the results of the 20.5 degree angle of attack calculation negates this conclusion. Vortex bursting was not evident over the wing at 30 degrees angle of attack.

Chapter I

Introduction

1.1 Problem Statement

To determine if vortex paneling methods can compute the vortex breakdown that occurs over a delta wing at high angles of attack.

1.2 Motivation for Research

The design of modern aircraft combines both analytical and experimental testing. As more powerful computers emerge, the usefulness and applicability of computer codes to predict the fluid characteristics over airfoils has increased. As aircraft operate in the high angle of attack regimes, the flow field becomes quite complex and is dominated by vortex-flow effects. The aerodynamic challenges this brings are expected to increase, as designers try to solicit the advantages of this flow. The ability to compute this complex airflow would facilitate the design process and reduce the costs associated with development.

1.3 Background

A grasp of what is vortex breakdown and how will it be determined numerically needs to be addressed. Within the

context of this effort, the terms "vortex breakdown" and "vortex bursting" are used synonymously and are restricted in reference to the fluid flow over delta wings. Ekaterinaris and Schiff describe vortex breakdown:

> An increase in the angle of attack strengthens the vortices (generated along the leading edges) until eventually a sudden change occurs in the nature of the cores. This sudden change is know as vortex breakdown. Vortex breakdown involves a transition of the vortex core from jet-like to a wake-like flow. (2:1)

Hitzel defines vortex breakdown as "... a rapid change of the vortex structure and a corresponding diminishing of the induced suction forces" (3:73). O'Neil, Barnett, and Louie describe the breakdown effect with respect to the leading-edge vortex, "... the well-defined leading-edge vortex degenerated rapidly into a substantially larger, more diffuse vortical flow region with relatively mild gradients" (7:220).

Several attempts have been made to compute the leading-edge vortex breakdown that occurs over delta wings at high angle of attack. Hitzel investigated this phenomena using Euler-methods. He found that the Euler-methods simulated the leading-edge vortices despite the neglect of viscous effects. He states,

> Often vortex-breakdown was supposed to be triggered by viscous effects. However as experiments showed, breakdown is almost independent of viscous effects...Breakdown is triggered by adverse pressure-gradients which decelerate the axial flow. By the demands of continuity and the conservation of

> momentum the vortex-core is forced to widen considerably...and the suction-peaks producing the nonlinear lift will decline.

In his calculations, Hitzel was able to compute the leading-edge vortex breakdown that provided "good agreement" with experiments. However, his solutions "exhibit very high total pressure losses in the vortex-core", and he attributes these losses to numerical errors introduced by the descretization of the mesh. Furthermore, there were two vortex diminishing effects. One of these causes was the decreasing geometrical resolution of the vortex wake. As the vortices leave the wing, they flow into the coarser outer part of the computational domain. The other vortex diminishing effect was caused by the downstream boundary conditions. Hitzel states, "Any boundary condition impose some constant free-flow conditions, (therefore) the vort : almost must cease to exist at the boundary." (3:73-83)

O'Neil, Barnett, and Louie also investigated vortex breakdown over delta wings using Euler-methods. They echo Hitzel's remarks that vortex breakdown is governed primarily by inviscid factors. They found in their computations that

> the well-defined leading-edge vortex degenerated rapidly into a substantially larger, more diffuse vortical flow region with relatively mild gradients...The occurrences of such breakdown-like events in the Euler solutions were found to have definite trends, and were clearly not a result of arbitrary numerical coincidence.

They developed a method to identify the location of vortex breakdown. At the onset of vortex breakdown, the locus of maximum swirl angle, falls in toward the vortex axis. This identifies the point of vortex breakdown, or shear-layer collapse. However, they too experienced the numerical dissipation induced by the artificial viscosity, which is common to all Euler codes. (7:218-226)

1.4 Scope of Development

The effort used the vortex panel method developed by Mracek. (6:11-100) Panel methods are used to describe inviscid, potential-flow aerodynamics. The method is a hybrid of vortex paneling methods, which describe the surface, and vortex lattice methods, which are used to model the wake. The advantages over Euler-methods are numerous. Hitzel states,

> "In Euler-calculations usually the start conditions already introduce vorticity... A proper natural evaluation of the vorticity however should start from zero evolving to the flight-velocity to simulate the real time-dependent build-up of the flow." (3:75)

This was performed within the panel method employed by starting the fluid flow impulsively. This method has a continuously developing wake that is not bound by a computational domain, or mesh. This eliminates the vortex diminishing effects and the initial induced vorticity over the

surface as found in Euler-codes. This method also allows for the ability to apply and move control surfaces on the airfoil, and account for roll-, pitch-, and yaw-rates.

A two-dimensional vortex panel method was used to investigate two separate splitting algorithms of the wake. The wake will be modeled as a vortex sheet composed of discrete vortex cores. As the wake cores are convected downstream, the distance between adjacent cores i ease. In order to sustain a continuous distribution of wake cores, additional cores are added between those that have moved sufficiently apart. The strengths of the added cores are determined from the conservation of circulation within the wake. This provided a splitting model to be used in the three-dimensional vortex panel method. Similar to the two-dimensional modeling of the wake, the three-dimensional representation of the vortex sheet used discrete vortex cores, although, they are of finite length due to the added dimension. An investigation into weighting values on the Kutta condition for the leading edge was accomplished to create the correct flow condition off the leading edge. The wake data was organized into a finite element methodology. This reduced the amount of computer memory and computational time required for a given calculation. An analysis is then presented on a unit aspect ratio delta wing, comparing the results at 20.5 and 30 degrees angle of attack.

Chapter II

Two-dimensional Model

2.1 Introduction

A two-dimensional vortex panel method was used to investigate two different wake splitting algorithms. The superior of the two models was then extended into the three-dimensional vortex panel method. A panel method describes potential-flow aerodynamics. The surface of the airfoil is modeled using segments on which the surface vorticity is linearly varying. The wake was modeled as a vortex sheet composed of vortex cores. As the cores are convected downstream, they disperse and move further apart. In order to model a continuous wake, additional cores are added between those cores that have moved sufficiently apart. This was termed wake splitting, as the strength of the new core is dependent on the two adjacent cores.

2.2 Two-Dimensional Vortex Panel Method

A two-dimensional vortex panel method was used to investigate the wake splitting because of its simplicity and corresponding relationship to the three-dimensional vortex panel method. In both cases, a potential flow model is used to describe the flow. The velocity is described as:

$$\overline{V} = \nabla\phi \tag{2-1}$$

The continuity equation for incompressible flow is:

$$\nabla\overline{V} = 0 \tag{2-2}$$

Subsituting in for the velocity potential yields Laplaces equation.

$$\nabla^2\phi = 0 \tag{2-3}$$

The vortex distribution was choosen such that Laplaces equation was always satisified, therefore, only the boundary conditions needed to be investigated.

For the two-dimensional model, the surface of the airfoil was modeled using line segments, or panels, on which the surface vorticity is linearly varying. Time was partitioned into time steps and equated to the average length of the panels representing the surface. Both the chord and freestream velocity was nondimensionalized. A wake was generated off the trailing edge and was modeled as a vortex sheet composed of discrete vortex cores. At each new time step a new trailing edge core was generated. The wake cores were then convected at the local particle velocity to preserve a pressure free wake position.

The total velocity of the potential flow around a body can be written in terms of the free-stream velocity and the disturbance velocity.

$$\overline{V} = \overline{V}_{fs} + \overline{V}_{d} \tag{2-4}$$

The disturbance velocity is the change in velocity due to the presence of the physical body and the velocity induced by the wake.

$$\overline{V}_{d} = \overline{V}_{body} + \overline{V}_{wake} \tag{2-5}$$

The no penetration condition on the surface was used to solve for the vorticity on the airfoil.

$$\overline{V} \cdot \hat{n} = 0 \quad \text{(on the surface)} \tag{2-6}$$

where $\hat{n}$ is the unit normal vector to the surface.

The velocity induced at any location in space by a point vortex is given by: (4:381)

$$dV = \frac{d\Gamma}{2\pi r}\hat{e}_{\theta} \tag{2-7}$$

Figure 1 presents a panel where the vorticity is linearly varying.

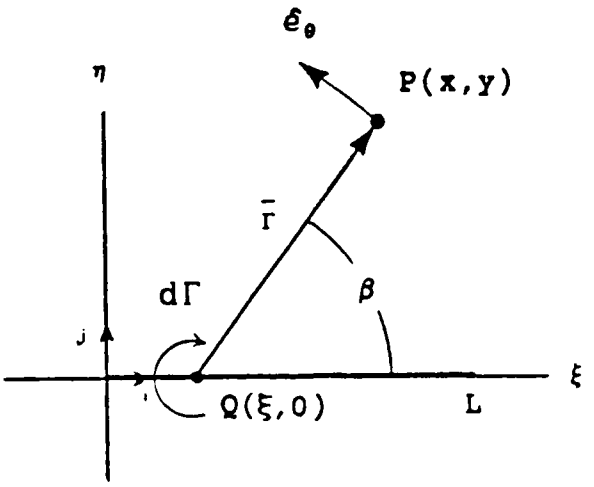

Figure 1. Two-Dimensional Vortex Panel

Where the linearly varying vortex distribution is provided by:

$$\Omega(\xi) = G_1\left(1 - \frac{\xi}{L}\right) + G_2\frac{\xi}{L} \tag{2-8}$$

Where G_1 and G_2 are the vortex strengths at the endpoints. It is known that

$$d\Gamma = \Omega(\xi)d\xi \tag{2-9}$$

Therefore, the total velocity induced by a vortex panel is determined by integrating along the length of the panel:

$$\bar{V}_p = \int_0^L \frac{\Omega(\xi)d\xi}{2\pi r}\hat{e}_\theta \tag{2-10}$$

Using a right-handed coordinate system yields:

$$\hat{e}_\theta = -\sin\beta\hat{i} + \cos\beta\hat{j} \tag{2-11}$$

$$r = \sqrt{(x-\xi)^2 + y^2}$$

where,

$$\sin\beta = \frac{y}{r} \qquad \cos\beta = \frac{x-\xi}{r} \tag{2-12}$$

Thus,

$$\bar{V}_p = \int_0^L \frac{\Omega(\xi)}{2\pi}\left[\frac{y}{(x-\xi)^2 + y^2}\hat{i}\right]d\xi - \int_0^L \frac{\Omega(\xi)}{2\pi}\left[\frac{x-\xi}{(x-\xi)^2 + y^2}\hat{j}\right]d\xi \tag{2-13}$$

By normalizing the length of the panel to one, the vortex strength along the panel becomes:

$$\Omega(\xi) = G_1(1-\xi) + G_2\xi \tag{2-14}$$

Substituting for $\Omega(\xi)$:

$$\bar{V}_p = \frac{1}{2\pi}\int_0^1 [G_1(1-\xi)+G_2\xi]\left[\frac{y\hat{i}-(x-\xi)\hat{j}}{(x-\xi)^2+y^2}\right]d\xi \tag{2-15}$$

or,

$$\begin{aligned}\bar{V}_p = {} & \frac{G_1}{2\pi}\int_0^1 \frac{(1-\xi)[y\hat{i}-(x-\xi)\hat{j}]}{(x-\xi)+y^2}d\xi \\ & + \frac{G_2}{2\pi}\int_0^1 \frac{y\xi\hat{i}-\xi(x-\xi)\hat{j}}{(x-\xi)^2+y^2}d\xi\end{aligned} \tag{2-16}$$

This supplies four integral equations that need to be solved:

$$\begin{aligned}\bar{V}_p = {} & V_{px}|_{G_2=0}G_1\hat{i} + V_{py}|_{G_2=0}G_1\hat{j} + \\ & V_{px}|_{G_1=0}G_2\hat{i} + V_{py}|_{G_1=0}G_2\hat{j}\end{aligned} \tag{2-17}$$

where,

$$
\begin{aligned}
V_{px}|_{G_2=0} &= \frac{1}{2\pi}\int_0^1 \frac{(1-\xi)y}{(x-\xi)^2+y^2}d\xi \\
V_{py}|_{G_2=0} &= \frac{1}{2\pi}\int_0^1 \frac{(1-\xi)(\xi-x)}{(x-\xi)^2+y^2}d\xi \\
V_{px}|_{G_1=0} &= \frac{1}{2\pi}\int_0^1 \frac{y\xi}{(x-\xi)^2+y^2}d\xi \\
V_{py}|_{G_1=0} &= \frac{1}{2\pi}\int_0^1 \frac{\xi(\xi-x)}{(x-\xi)^2+y^2}d\xi
\end{aligned}
\qquad (2\text{-}18)
$$

Solving these integrals yields:

$$
\begin{aligned}
V_{px}|_{G_2=0} &= \frac{1}{2\pi}\left[(1-x)\Delta\theta + \frac{y}{2}\ln R\right] \\
V_{py}|_{G_2=0} &= \frac{1}{2\pi}\left[\frac{(1-x)}{2}\ln R + y\Delta\theta - 1\right] \\
V_{px}|_{G_1=0} &= \frac{1}{2\pi}\left[x\Delta\theta + \frac{y}{2}\ln R\right] \\
V_{py}|_{G_1=0} &= \frac{1}{2\pi}\left[1 - y\Delta\theta + \frac{1}{2}x\ln R\right]
\end{aligned}
\qquad (2\text{-}19)
$$

where,

$$
\begin{aligned}
\Delta\theta &= \tan^{-1}\left(\frac{x}{y}\right) - \tan^{-1}\left(\frac{x-1}{y}\right) \\
\ln R &= \ln\left[\frac{(x-1)^2+y^2}{x^2+y^2}\right]
\end{aligned}
\qquad (2\text{-}20)
$$

There are two singularities: x=0, y=0, and x=1, y=0. Other regions that deserve careful consideration are when y=0, and x<0, 0<x<1, and x>1. The results of these limits are:

$$\begin{aligned} x<0 \quad y=0 \quad \Delta\theta=0 \\ x>1 \quad y=0 \quad \Delta\theta=0 \\ 0<x<1 \quad y\to 0^{+} \quad \Delta\theta=\pi \\ 0<x<1 \quad y\to 0^{-} \quad \Delta\theta=-\pi \end{aligned} \tag{2-21}$$

A simple coordinate transform was used when the panel did not lie on the axis. Where,

$$\begin{Bmatrix} \hat{i} \\ \hat{j} \end{Bmatrix} = \begin{bmatrix} \cos\gamma & \sin\gamma \\ -\sin\gamma & \cos\gamma \end{bmatrix} \begin{Bmatrix} \hat{I} \\ \hat{J} \end{Bmatrix} \tag{2-22}$$

The velocity induced on a point in space by a panel can be considered as:

$$\begin{aligned} \overline{V}_p &= V_x\hat{i} + V_y\hat{j} \\ &= [V_x \quad V_y] \begin{Bmatrix} \hat{i} \\ \hat{j} \end{Bmatrix} \\ &= [V_x \quad V_y] \begin{bmatrix} \cos\gamma & \sin\gamma \\ -\sin\gamma & \cos\gamma \end{bmatrix} \begin{Bmatrix} \hat{I} \\ \hat{J} \end{Bmatrix} \end{aligned} \tag{2-23}$$

where,

$$V_x = V_{px}|_{G_2=0} G_1 + V_{px}|_{G_1=0} G_2$$
$$V_y = V_{py}|_{G_2=0} G_1 + V_{py}|_{G_1=0} G_2 \qquad (2\text{-}24)$$

The vector dot product with the outward normal, required for the no-penetration condition, was then performed on this component of the velocity.

The surface of the airfoil consisted of numerous panels joined together at their endpoints as illustrated in Figure 2. The endpoints were termed nodes. For a closed surface, there are the same number of nodes as there are panels. The surface vorticity was constrained to be continuous, i.e. the G_1 of a one panel was equal to the G_2 of the preceding panel. Therefore, each node has a single vortex strength (G).

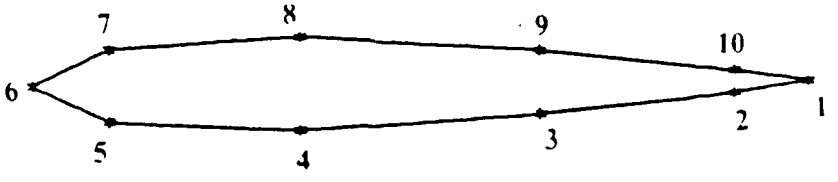

Figure 2. Vortex Panel Modeling of a NACA0012 Airfoil

The no penetration condition was only solved at the midpoints of each panel, or control points. Each panel has an influence at every control point. When the vector dot product is performed with the outward normal, this provides a number of equations equal to the number of panels describing the surface. This results in an influence matrix [A]. The only unknowns are the vorticity at each node. Hence,

$$[A]\{G\} = [\bar{V}_{body}] \tag{2-25}$$

where $[\bar{V}_{body}]$ is the perturbation in velocity that the body produces at each control point.

The wake consists of vortex cores that have been generated at the trailing edge, then convected downstream at the local particle velocity. The strengths of all the wake cores are known except for the trailing edge core. Its strength was determined from:

$$\Gamma_{total} = 0 \tag{2-26}$$

or,

$$\Gamma_c + \Gamma_{wing} + \Gamma_{wake} = 0 \tag{2-27}$$

where,

$$\Gamma_{wing} = \int_{body} \bar{\Omega} \cdot \hat{n}\, ds = \sum G_i l_i = [l]\{G\} \tag{2-28}$$

l_i = distance between control points

Γ_{wake} = $\sum$ circulation of the remaining wake cores

Γ_c = circulation strength of the trailing edge core

$= -\Gamma_{wake} - \Gamma_{wing}$

$= -\Gamma_{wake} - [l]\{G\}$

The $[l]$ is a row matrix containing the distance between the control points of adjacent panels and $\{G\}$ is a column matrix comprising the vorticity strength at each node.

The wake also influences the velocity at the control points. The vortex sheet was modeled as a set of discrete cores. The velocity induced at any point in space by a vortex core is determined from: (4:381)

$$\bar{V} = \frac{\Gamma}{2\pi r} \hat{e}_\theta \tag{2-29}$$

where r is the distance from the vortex core to the point in question.

The trailing edge core also induce velocities at the control points, given by:

$$\overline{V}_{c_\ell} = \frac{\Gamma_c}{2\pi r_\ell}\hat{e}_\theta \tag{2-30}$$

where,

r_ℓ = distance from trailing edge core to a control point

The vector dot product with the outward normal vector at each control point can be performed. The result is the disturbance the trailing edge core has on the velocity at the control points.

$$\{c\}\Gamma_c = [\overline{V}_c] \tag{2-31}$$

The matrix {c} is comprised of the distances from the trailing edge core to each control point. The no penetration condition is therefore,

$$[A]\{G\} + \{c\}\Gamma_c + \overline{V}_{wake}\cdot\hat{n} + \overline{V}_{fs}\cdot\hat{n} = 0 \tag{2-32}$$

Substituting for the trailing edge core strength,

$$[[A]-\{c\}[l]]\{G\} = \{c\}\Gamma_{wake} - \overline{V}_{wake}\cdot\hat{n} - \overline{V}_{fs}\cdot\hat{n} \qquad (2\text{-}33)$$

or,

$$[A']\{G\} = [b'] \qquad (2\text{-}34)$$

where,

$$[A'] = [A]-\{c\}[l] \qquad (2\text{-}35)$$
$$[b'] = \{c\}\Gamma_{wake} - \overline{V}_{wake}\cdot\hat{n} - \overline{V}_{fs}\cdot\hat{n}$$

The only unknowns are the strength of the vorticity at the nodes, however, imposing the Kutta condition requires that the strength of the vorticity at the trailing edge is zero, or $G_1=0$. Therefore, the number of equations now exceed the number of unknowns. The method of solution was a reduction in the square of the errors. This is given by:

$$[A']^T[A']\{G\} = [A']^T[b'] \qquad (2\text{-}36)$$

This matrix equation can be solved using a number of different numerical methods techniques available. Once the strengths of the vorticity are known at the nodes, the

strength of the trailing edge core is calculated. The wake cores are then convected at the local particle velocity to produce a pressure free surface.

2.3 Wake Splitting Algorithms

The wake cores are convected at the local particle velocity. The velocity induced on a core by itself is infinite. Since this is unrealistic, there was a small area around each wake core for which that core had no influence.

Once the wake cores move downstream, large distances are created between adjacent cores. In an attempt to model the diffusion of the vorticity and to sustain a continuous wake, wake cores will be added between those that have moved sufficiently far apart. This is illustrated in Figure 3.

Two different wake splitting algorithms were investigated. In each case, cores are divided into smaller ones as the wake forms. The first method of wake splitting was similar to that investigated by Mook, et al (4:4). Once the distance between two adjacent cores reached a prescribed distance, $\sqrt{2}dt$, a core would be added and the two bounding cores reduced in strength. This distance was choosen in order to sustain approximately the same distance between every core. The strength of the added core would be given by:

$$\Gamma_{added} = \frac{1}{3}\Gamma_n + \frac{1}{3}\Gamma_{n+1} \tag{2-37}$$

and then

$$\begin{aligned} \Gamma_n &= \frac{2}{3}\Gamma_n \\ \Gamma_{n+1} &= \frac{2}{3}\Gamma_{n+1} \end{aligned} \tag{2-38}$$

If additional cores were required to be added on both sides of a wake core, the strength of the added cores would be:

$$\begin{aligned} \Gamma_{added_1} &= \frac{1}{3}\Gamma_{n-1} + \frac{1}{4}\Gamma_n \\ \Gamma_{added_2} &= \frac{1}{4}\Gamma_n + \frac{1}{3}\Gamma_{n+1} \end{aligned} \tag{2-39}$$

where,

$$\begin{aligned} \Gamma_{n-1} &= \frac{2}{3}\Gamma_{n-1} \\ \Gamma_n &= \frac{1}{2}\Gamma_n \\ \Gamma_{n+1} &= \frac{2}{3}\Gamma_{n+1} \end{aligned} \tag{2-40}$$

In this way, the total circulation of the wake remained constant throughout the splitting process. Figure 3 illustrates this procedure. A row of four nodes are represented by the darkened circles at an arbitrary time, τ. At $\tau + \delta\tau$, they are convected at the local particle velocity to their new respective positions. Enough distance has been created between the last three nodes to require splitting. This necessitates the addition of two wake nodes represented by the open circles. The strengths of the wake nodes are then determined by the equations 2-37 through 2-40.

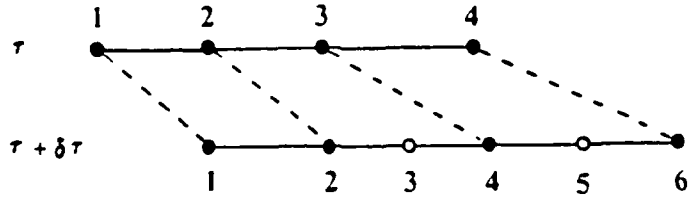

Figure 3. Basic Two-Dimensional Wake Splitting

The second algorithm was an extension of the first. The wake cores would be convected at the local particle velocity to establish their new respective positions. If the distance between any adjacent cores was sufficient to warrant splitting, a new core would be added between them at

their original positions before convection. The strengths of which are given by equations 2-37 through 2-40. The entire wake would then again be convected and the distances between adjacent cores rechecked. This would continue until all the distances between adjacent cores were within the specified limit. This method is illustrated in Figure 4.

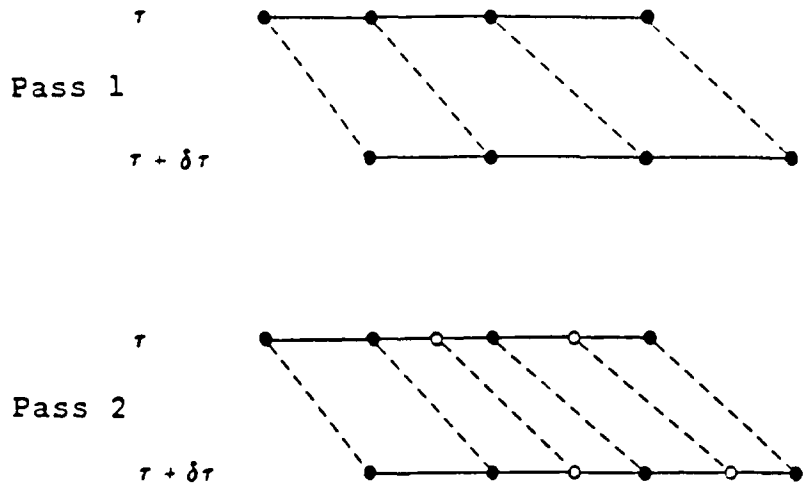

Figure 4. Enhanced Two-Dimensional Wake Splitting

2.4 Results

The airfoil investigated was a NACA0012 airfoil. The following equation was used to determine the location of the nodes. (1:113)

REPORT DOCUMENTATION PAGE

Form Approved
OMB No. 0704-0188

1. AGENCY USE ONLY (Leave blank)	2. REPORT DATE	3. REPORT TYPE AND DATES COVERED
	December 1990	

4. TITLE AND SUBTITLE

VORTEX BURSTING OVER A UNIT ASPECT RATIO DELTA WING USING VORTEX-PANEL METHODS

5. FUNDING NUMBERS

6. AUTHOR(S)

Donald A. Lorey, Captain, USAF

7. PERFORMING ORGANIZATION NAME(S) AND ADDRESS(ES)

Air Force Institute of Technology,
WPAFB OH 45433-6583

8. PERFORMING ORGANIZATION REPORT NUMBER

AFIT/GAE/ENA/90D-14

9. SPONSORING/MONITORING AGENCY NAME(S) AND ADDRESS(ES)

10. SPONSORING/MONITORING AGENCY REPORT NUMBER

11. SUPPLEMENTARY NOTES

12a. DISTRIBUTION/AVAILABILITY STATEMENT

Approved for public release:
distribution unlimited

12b. DISTRIBUTION CODE

A unit aspect ratio delta wing is analyzed to determine if a unsteady vortex panel method can calculate the vortex bursting of the vortex developed along the leading-edge. A two-dimensional vortex panel method is used to investigate wake splitting schemes of the vortex cores that comprise the vortex sheet, or wake. The worthier of the splitting methods is later implemented into the three-dimensional wake. The weighting values of the Kutta equations are investigated for the leading-edges, and are determined to be problem specific. An alternative approach to the management of the wake data is presented and implemented. The delta wing is then analyzed for 20.5 and 30 degrees angle of attack. The panel method produced a perturbation and enlargement in the wake at the two-thirds chord position over the wing at 30 degrees angle of attack, indicative of vortex breakdown. However, a qualitative comparison with the results of the 20.5 degree angle of attack calculation negates this conclusion. Vortex bursting was not evident over the wing at 30 degrees angle of attack.

14. SUBJECT TERMS

Vortex Bursting, Vortex Breakdown,
Vortex Panel Methods, Vortex Lattice Methods

15. NUMBER OF PAGES

66

16. PRICE CODE

17. SECURITY CLASSIFICATION OF REPORT	18. SECURITY CLASSIFICATION OF THIS PAGE	19. SECURITY CLASSIFICATION OF ABSTRACT	20. LIMITATION OF ABSTRACT
Unclassified	Unclassified	Unclassified	UL

$$y(x) = \pm\frac{0.12}{0.2}\left(0.2969\sqrt{x} - 0.1260x - 0.3516x^2 + 0.2843x^3 - 0.1015x^4\right) \quad (2\text{-}41)$$

where,

$$x = 0.5 + 0.5\cos(\theta) \quad (2\text{-}42)$$

Where θ is incremented from 0 to 2π by:

$$\Delta\theta = \frac{2\pi}{\text{number of panels}} \quad (2\text{-}43)$$

This was used to capture the increased curvature of the leading edge.

The airfoil was modeled using 200 panels, at an angle of attack of 5 degrees, and was impulsively started. The chord was set equal to one, and the time step was 0.01, since this was the approximate average length of the panels. Figures 5 and 6 compare the vortex sheet at time steps of 25, 50, 75, and 100. The vortex cores are not shown. Instead a curve connecting consecutive cores is provided as a representation of the vortex sheet. Notice there is no visible difference in the wake for these times. Likewise, Figures 7 and 8 show the position of the wake at 125 and 150

time steps. A small difference is noticeable at 150 time steps. Both algorithms produced essentially the same results. However, the enhanced splitting method required approximately 25 percent more computational time. This added computational requirement would increase as the calculation was continued. The primary cause was the added calculations required to compute the local velocity twice for the entire wake each time step. The enhanced splitting algorithm therefore did not provide a substantial improvement to warrant its use in the three-dimension paneling method.

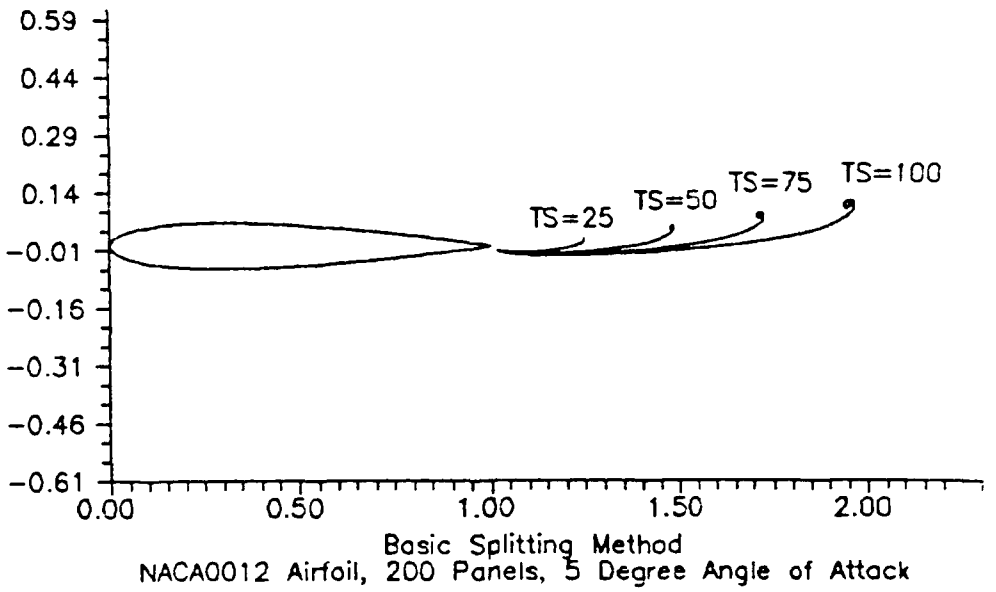

Figure 5. Wake Formation Using the Basic Splitting Algorithm

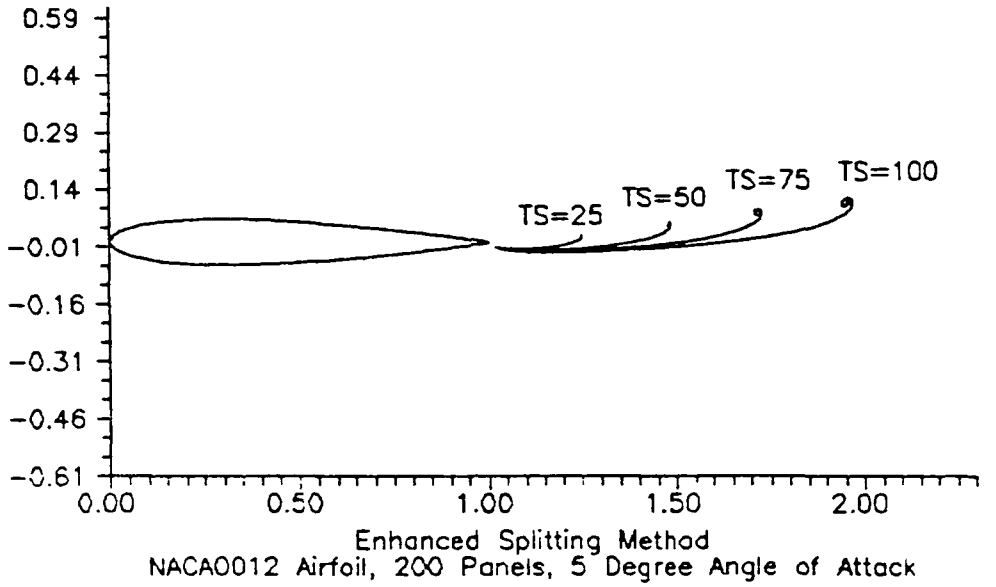

Figure 6. Wake Formation Using the Enhanced Splitting Algorithm

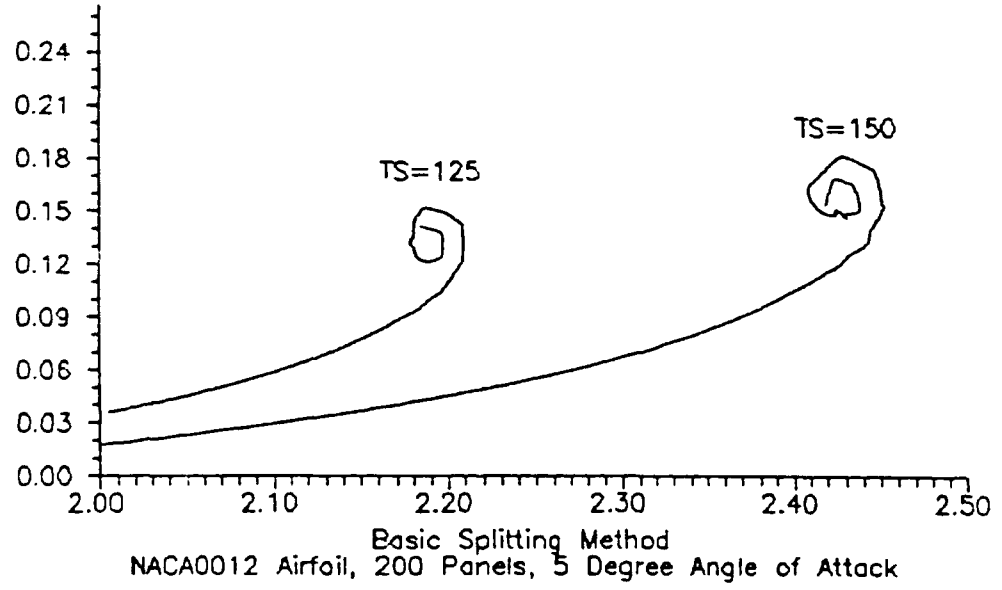

Figure 7. Downstream Wake Formation Using the Basic Splitting Algorithm

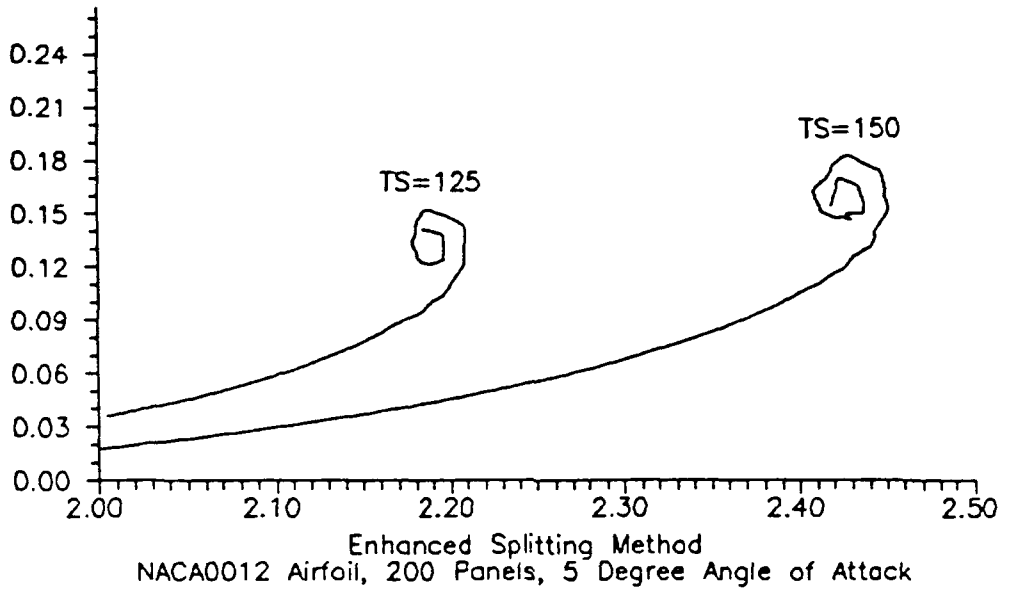

Figure 8. Downstream Wake Formation Using the Enhanced Splitting Algorithm

Chapter III

Three-dimensional Model

3.1 Introduction

A three-dimensional vortex panel method was used to investigate the vortex generated over a unit area aspect ratio delta wing at high angle of attack. The method was developed by Mracek and uses triangular elements, or panels, on which the surface vorticity is piecewise linearly varying. Quadratically varying vortex cores are placed at the edges in order to generate a nonzero vorticity at the edges. The wake was modeled as a vortex sheet, composed of discrete vortex cores, which emanate from the edges of the surface. (5:Chapter 2)

The presentation of the complete aerodynamic model is too extensive to present here. The solution method used was a minimization in the square of the errors. This permited the use of weighting values to accentuate, or deemphasize certain equations with respect to the other equations. The weighting value for the Kutta equations was investigated for the leading edges.

An alternate approach to Mracek's modeling of the wake was performed. The new method is analogous to a finite element technique, using nodes and elements. The nodes are

convected at the local particle velocity. The splitting algorithm was extended from the two-dimensional model and applied to the three-dimensional wake.

3.2 Aerodynamic Model

The three-dimensional vortex panel method was provided by Mracek. The method uses triangular panels, or elements, on which the surface vorticity is piecewise linearly varying, to model the lifting surface. The vertex of each triangular element was termed a node. Additional vortex cores are placed at the edges in order to generate a nonzero vorticity at the edges. The wake was modeled as a vortex sheet, composed of discrete vortex cores, or vortex lattice, which emanated from the edges of the wing.

Typical to vortex paneling methods, there exists more equations than unknowns. The unknowns to the problem are the strength of the surface vorticity at the nodes, and the constants of integration associated with the surface edge cores. Again, Laplaces equation was satisfied, and only the boundary conditions were addressed. The resulting matrix equation was:

$$\begin{bmatrix} A+C & D \\ B & 0 \\ E & F \\ J & 0 \\ K & L \end{bmatrix} \begin{Bmatrix} \Omega \\ G \end{Bmatrix} = \begin{bmatrix} U-W \\ 0 \\ 0 \\ 0 \\ P \end{bmatrix} \tag{3-1}$$

This equation is the culmination of four sets of equations, each of which are discused separately.

The no penetration conditions at the midpoint of each element, or control points, is given by:

$$\overline{V} \cdot \hat{n} = 0 \quad \text{on the surface} \tag{3-2}$$

Each element has an influence in the velocity at every control point on the surface. The result was an influence matrix, [A].

$$[A+C \quad D] \begin{Bmatrix} \Omega \\ G \end{Bmatrix} = \{U-W\} \tag{3-3}$$

Also included was the influence of the edge cores which are dependent on the surface vorticity, and the velocity induced by the wake.

The flow field must also satisfy the continuity equation for incompressible flow.

$$\operatorname{div} \bar{V} = 0 \tag{3-4}$$

A vector field, A, is chosen such that

$$\bar{V} = \operatorname{curl} \bar{A} \tag{3-5}$$

Thus, the continuity equation becomes:

$$\operatorname{div}(\operatorname{curl} \bar{A}) = 0 \tag{3-6}$$

The vorticity in the flow field is defined as:

$$\bar{\Omega} = \operatorname{curl} \bar{V} \tag{3-7}$$

Because the freestream is irrotational, the vorticity was defined as the curl of the disturbance velocity only. The disturbance velocity can then be found by solving the following equation:

$$\bar{\Omega} = -\nabla^2 \bar{A} \tag{3-8}$$

Green's theorem yields:

$$\bar{A}(\bar{r}, t) = \frac{1}{4\pi} \int\int\int_R \frac{\bar{\Omega}(\bar{r}, t)}{|\bar{r} - \bar{s}|} d\tau \tag{3-9}$$

From Karamcheti, if the vorticity is contained within a short distance, ϵ, of the surface, as ϵ approaches zero, the product of $|\bar{\Omega}|$ and ϵ remains constant, and $\bar{\Omega}$ becomes tangent to the surface (3:530-532). Therefore,

$$\bar{\gamma}(\bar{s}) = \lim_{|\bar{\Omega}|\to\infty,\,\epsilon\to 0} \bar{\Omega}\epsilon \tag{3-10}$$

Rewriting the volume integral as a surface integral:

$$\bar{A}(\bar{r}) = \frac{1}{4\pi}\int\int_S \frac{\bar{\gamma}(\bar{s})}{|\bar{r}-\bar{s}|}d\sigma \tag{3-11}$$

Since the disturbance velocity is the curl of the vector field A, and the divergence of the curl of a vector is identically zero, any vector field that represents the surface vorticity will satisfy the continuity equation as long as:

$$\mathrm{div}\,\bar{\gamma} = 0 \tag{3-12}$$

This divergenceless condition for the surface can be represented in matrix form by:

$$[B \quad 0]\begin{Bmatrix}\Omega\\ G\end{Bmatrix} = \{0\} \tag{3-13}$$

Quadratically varying cores are added to the edges of the lifting surface to either capture or create the vortex sheet. The circulation around the core is dependent on the vorticity of the neighboring vortex element. This is depicted in Figure 9.

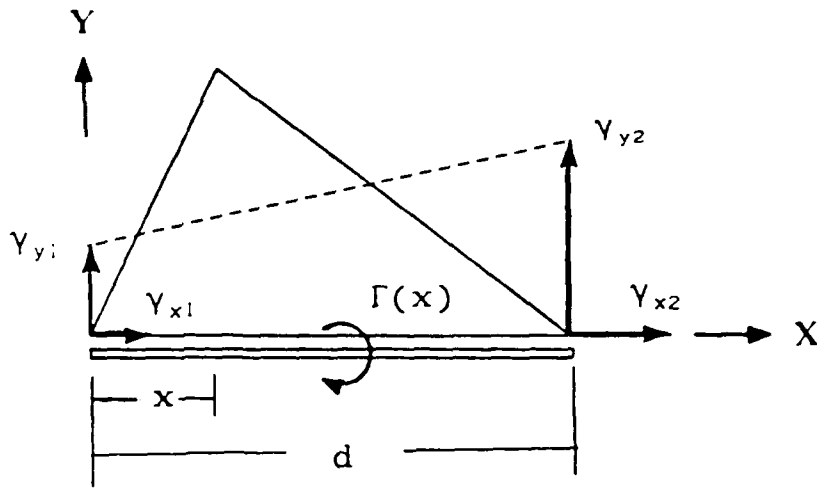

Figure 9. Edge Core and Edge Element

Along the edge of the element:

$$\gamma(x) = \frac{\gamma_{y2} - \gamma_{y1}}{d} x + \gamma_{y1} \qquad (3\text{-}14)$$

For the edge cores to be compatable with the vortex panel, the circulation is given by:

$$\frac{d\Gamma}{dx} = \gamma \tag{3-15}$$

Integration provides the circulation around the core.

$$\Gamma(x) = \left[\frac{\gamma_{y2} - \gamma_{y1}}{d}\right]\frac{x^2}{2} + \gamma_{y1}x + G \tag{3-16}$$

where G is a constant of integration. In order to make the circulation continuous in strength around the body, two adjoining edge cores must have the same circulation at the connection. Additionally, the circulation around the cores are continuous through the first derivative at the juncture. These compatibility equations, in matrix form, are given by:

$$\begin{bmatrix} E & F \\ J & O \end{bmatrix}\begin{Bmatrix} \Omega \\ G \end{Bmatrix} = \{O\} \tag{3-17}$$

The final matrix equation is the Kutta equation. The Kutta condition was imposed only at the nodes of the surface along the edges. This was given by:

$$[K \quad L]\begin{Bmatrix} \Omega \\ G \end{Bmatrix} = \{P\} \tag{3-18}$$

A more in-depth derivation is provided in the following section.

A weighting matrix was used to emphasize one equation with respect to the other equations. Hence,

$$\begin{bmatrix} A+C & D \\ w_1 B & 0 \\ w_2 E & w_2 F \\ w_3 J & 0 \\ w_4 K & w_4 L \end{bmatrix} \begin{Bmatrix} \Omega \\ G \end{Bmatrix} = \begin{bmatrix} U-W \\ 0 \\ 0 \\ 0 \\ w_4 P \end{bmatrix} \tag{3-19}$$

The weighting value applied to the divergenceless condition has little impact on the solution. The weighting value used for this condition was 50. The weighting value for the edge compatibility needed to be large because these conditions need to be imposed exactly. Therefore, the weighting value associated with the edge compatibility was set to 500. Along the trailing edge, the Kutta condition also needed to be satisfied. The weighting valued applied to the Kutta equation was set to 50. An investigation into the weighting value of the Kutta condition along the leading edge is presented in section 3.3.

Equation 3-19 can be expressed as:

$$[S]\begin{Bmatrix} \Omega \\ G \end{Bmatrix} = \{T\} \tag{3-20}$$

where,

$$[S] = \begin{bmatrix} A+C & D \\ w_1 B & 0 \\ w_2 E & w_2 F \\ w_3 J & 0 \\ w_4 K & w_4 L \end{bmatrix} \tag{3-21}$$

and

$$\{T\} = \begin{bmatrix} U-W \\ 0 \\ 0 \\ 0 \\ w_4 P \end{bmatrix} \tag{3-22}$$

The chosen method of solution was to minimize the sum of the squares of the errors. This is the solution of the following equation:

$$[S]^T[S]\begin{Bmatrix} \Omega \\ G \end{Bmatrix} = [S]^T\{T\} \tag{3-23}$$

3.3 Kutta Weighting Values

The Kutta condition states: (6:45-50)

$$\Delta C_p|_{edge} = 0 \tag{3-24}$$

where the pressure coefficient is defined as:

$$C_p = \frac{P - P_\infty}{\frac{1}{2}\rho U^2} \tag{3-25}$$

Using Bernoulli's equation for unsteady flow:

$$\left.\frac{\partial \phi}{\partial t}\right|_{\vec{R}} + \frac{V^2}{2} + \frac{P}{\rho} = H(t) \tag{3-26}$$

where $\vec{R}$ is the position vector of the point in an inertial reference frame.

The far-field boundary condition was that the velocity potential was not changing with respect to time. The pressure coefficient can then be written as:

$$C_p = \frac{1}{U^2}\left[V_\infty^2 - V^2 - 2\left.\frac{\partial \phi}{\partial t}\right|_{\vec{R}} \right] \tag{3-27}$$

Hence,

$$\begin{aligned}\Delta C_p &= C_{pl} - C_{pu} \\ &= V_\infty^2 - V_l^2 - 2\frac{\partial \phi_l}{\partial t}\bigg|_{\vec{r}} + 2\vec{V}_l \cdot \vec{V}_p \\ &\quad - V_\infty^2 - V_u^2 - 2\frac{\partial \phi_u}{\partial t}\bigg|_{\vec{r}} + 2\vec{V}_u \cdot \vec{V}_p\end{aligned} \tag{3-28}$$

The Kutta equation was imposed ideally at the trailing edge. This was performed by using a weighting value of 50 for the Kutta equations associated with the trailing edge nodes. Along the leading edges, however, a large pressure gradient exists. In order to capture this pressure gradient a large number of elements would be required. This was unachievable along the front of the wing using discrete points. Therefore the Kutta condition can not be satisfied ideally. Instead, since it was known that the wake will convect off the leading edge tangential to the wing surface, the Kutta condition was only imposed, in as much, to cause this effect. A weighting value was implemented on the Kutta equations associated with the leading edge nodes.

It was evident that the required weighting value for the Kutta equations was job dependent. Several unit area aspect ratio delta wings, modeled with various number of elements were analyzed. Initially, a delta wing, modeled with 20 rows of elements was investigated with Kutta weighting values of 0.2 and 0.5. The angle of attack was

20.5 degrees, and the computations were computed to 20 time steps, or one chord length of wake. The Kutta weighting value of 0.2 was not sufficient enough to establish the tangency condition. The value of 0.5 however, produced the satisfactory result. As a test to investigate if the 0.5 value was too excessive, another computation was performed using 0.45. This value proved inadequate, therefore, a calculation with a Kutta weighting value of 0.48 was performed producing the required tangency condition. A unit area aspect ratio delta wing was then modeled with 30 rows of elements, using the 0.48 Kutta weighting value. Again the problem was carried out to obtain one chord length of wake, or in this case, 30 time steps. For this calculation, the value of 0.48 was inadequate. The required Kutta weighting value for the 30 row delta wing was determined to be 0.5. The angle of attack was then increased to 30 degrees. Initially a value of 0.5 was used as the weighting value. This proved inappropriate and a value of 0.515 was needed for this increased angle of attack. No analytical, or empirical relationship could be derived to determine the appropriate weighting value for any job in general. This data is provided in Table 1.

Table 1. Kutta Weighting Value

No. of Rows	Angle of Attack	Kutta Weighting Value	Results
20	20.5	0.200	Insufficient
20	20.5	0.500	Over-constrained
20	20.5	0.450	Insufficient
20	20.5	0.480	Satisfactory
30	20.5	0.480	Insufficient
30	20.5	0.500	Satisfactory
30	30.0	0.500	Insufficient
30	30.0	0.515	Satisfactory

3.4 Wake Modeling

The wake was model as a vortex sheet comprised of discrete vortex cores. The fluid flow was started impulsively, therefore, initially there was no wake. Once the fluid was set into motion, vorticity was formed on the surface. With this quadratically varying vortex cores were developed along the edges. The movement of the wake was given by the no pressure jump condition. The pressure on the upper surface of the wake must equal the pressure on the lower surface of the wake. In order to satisfy this condition, the wake cores were convected at the local particle velocity. The cores new positions were given by:

$$\vec{r}(t+\Delta t) = \vec{r}(t)+\vec{V}_p\Delta t \qquad (3\text{-}29)$$

where,

$\vec{V}_p$ = local particle velocity

dt = time step

Once the cores have moved downstream, the flow field around the wing is changed. This required a new vortex distribution on the wing and edges. The strength of the wake was determine by the conservation of circulation.

$$\Gamma_{total} = 0 \qquad (3\text{-}30)$$

This procedure was performed throughout the calculation for each time step.

In order to simplify the wake, vortex cores are also used to model the wake parallel to the flow. The endpoints of which connect to the endpoints of the cores convected from the edges of the surface. This creates a quadrilateral, or wake element, consisting of four vortex cores connected at their endpoints. Figure 10, illustrates the development of the wake lattice. Where the cores connect are termed wake nodes. To satisfy the fact that the vortex cores that comprise the wake will be of constant strength, the core circulation will be the average value of the quadratically varying edge core. The quadrilateral bounds a

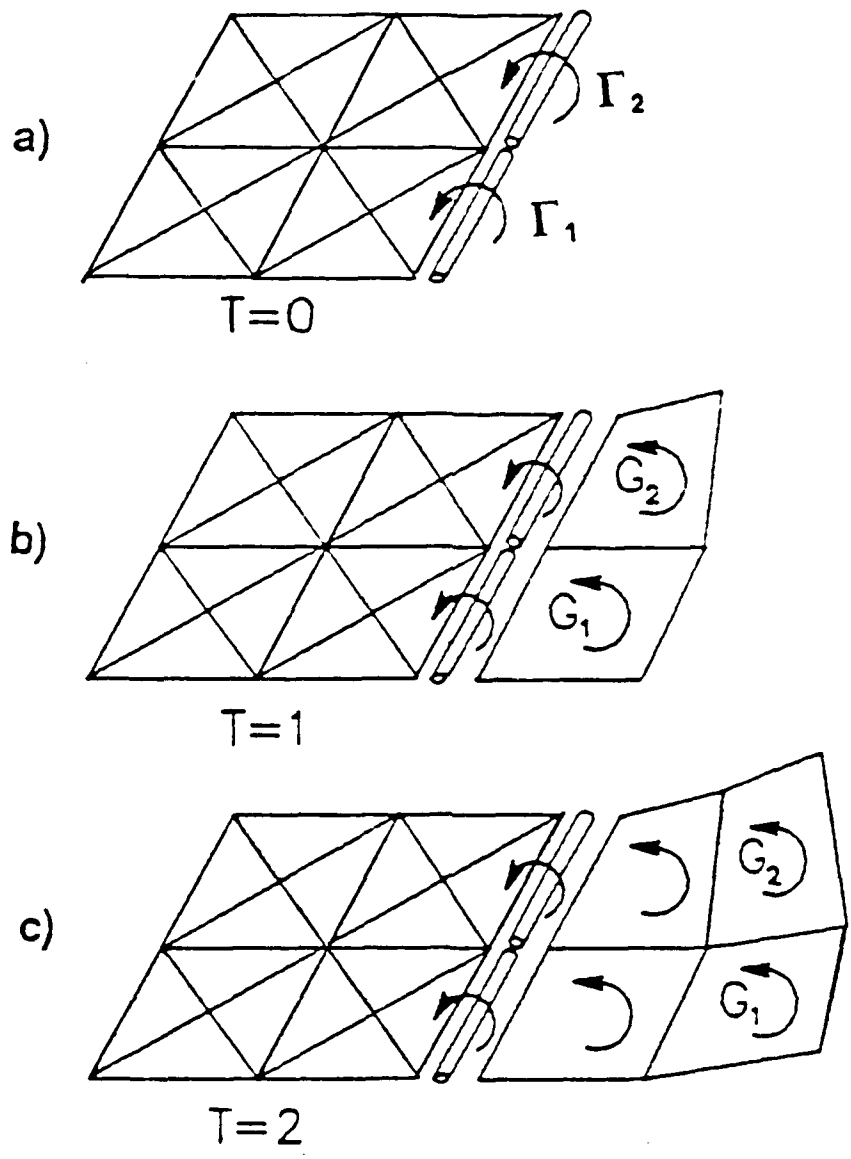

Figure 10. Development of the Wake Lattice

closed ring of circulation. Only the value of this circulation need be stored. The circulation of the quadratically varying edge core is given by:

$$\Gamma(x) = g_1\frac{x^2}{2} + g_2 x + g_3 \tag{3-31}$$

Therefore, the strength of the ring of circulation is given by:

$$G = \frac{\int_0^d \Gamma(x)dx}{d} = g_1\frac{d^2}{6} + g_2\frac{d}{2} + g_3 \tag{3-32}$$

As the calculation is carried out, the wake moves downstream and spreads out. As with the two-dimensional calculations, the wake was split in order to more closely model a continuous vortex sheet. The model was an extension of the one chosen in the two-dimensional model, although, now the wake was split in the spanwise direction. Once a wake element has deformed to warrant splitting, it was divided into two new wake elements, and two wake nodes are added. This is represented in Figure 11. The strength of the new wake elements are given by:

$$G'_{21} = G_{11} \quad G'_{22} = G_{12} \quad G'_{23} = G_{13}$$

$$G'_{31} = G_{21} \quad G'_{32} = \frac{1}{3}G_{21} + \frac{2}{3}G_{22} \qquad (3\text{-}33)$$

$$G'_{33} = \frac{2}{3}G_{22} + \frac{1}{3}G_{23} \quad G'_{34} = G_{23}$$

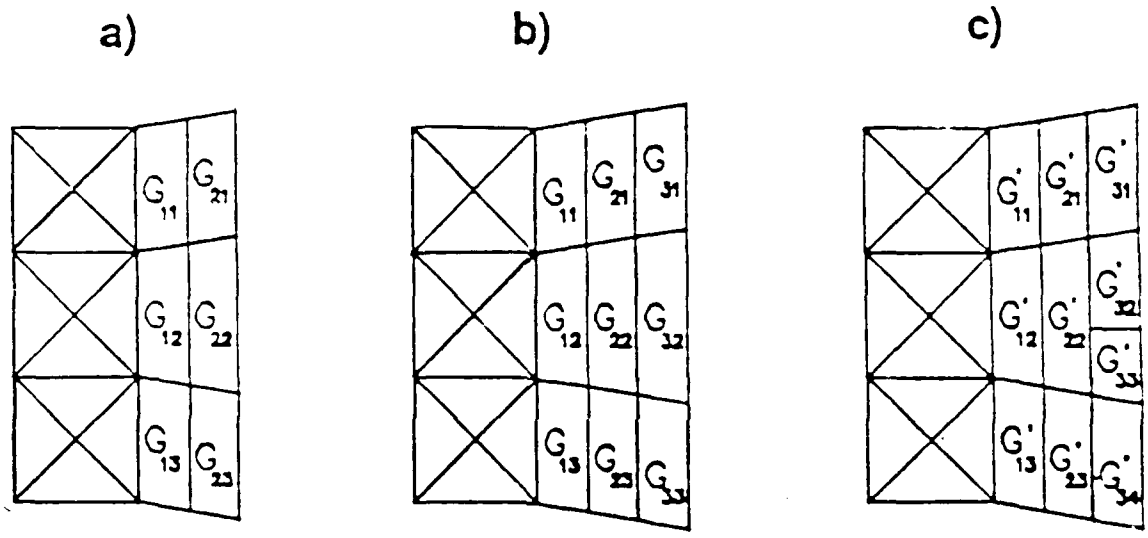

Figure 11. Splitting the Wake Lattice

Mracek performed the same splitting technique, but managed the wake data in a redundant manner. He considered each row of wake data as an independent wake entity, which necessitated the existence of two rows of wake nodes for each row of wake elements. To make the wake continuous, the

rows of wake elements would be attached. Assuming there were the same number of wake elements in two consecutive rows, the upstream row of wake nodes would correspond to the downstream row of wake nodes from the preceding row of elements. This redundancy required twice the amount of computer memory needed to describe the wake.

To eliminate the extra computer memory requirement, the bookkeeping of the wake used a finite element technique. The positions of the nodes, and the strengths of the circulations of the wake elements were only stored. Four nodes are associated with each wake element. Each node is shared by the surrounding elements. The wake can then be represented two-dimensionally. The nodes are numbered sequentially, starting at the upper left side and ending at the bottom right side of the wake. A matrix consisting of rows and columns was used to manage the circulation strength of the wake elements, Figure 12.

A two-dimensional representation of the wake is given by Figure 12. For the next time step this wake was used to in the solution process to solve for the vorticity distribution over the wing. It was also used, along with the new vorticity distribution, to determine the local particle velocity of the wake nodes. The wake nodes were then convected at the local particle velocity. A new row of wake nodes was added along the edges of the wing along with

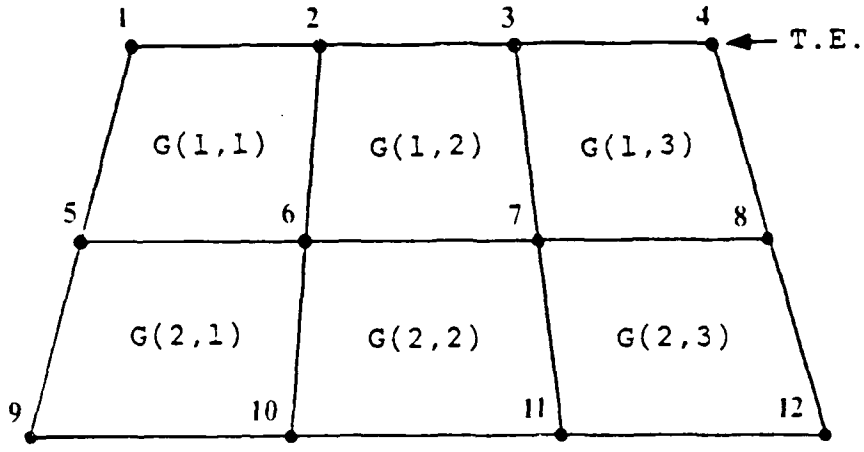

Figure 12. Finite Element Representation of the Wake

a new row of wake elements. The spanwise distance of the elements was then checked to see if splitting was necessary. Additional nodes and elements were added as required. This process starts with the last row of elements and proceeded upstream towards the wing. Once a row of elements was reached that does not require splitting and still contained its original number of elements, no further investigation into the spanwise distance of the elements was needed. This was based on the premise that the wake is continually diverging. The nodes and elements were then resequenced to conform to the previous numbering scheme, Figure 13.

As a check, two calculations using a unit aspect ratio

delta wing, modeled with 20 rows of elements, at an angle of attack of 20 degrees were performed each using one of the wake data management systems described above. The calculations were performed to 20 time steps. The finite element methodology was verified, computing the same wake mesh as Mraceks method. However, the finite element technique required less total memory, and computer time than the previous method employed. Therefore, this wake data management procedure was retained for the remainder of this effort.

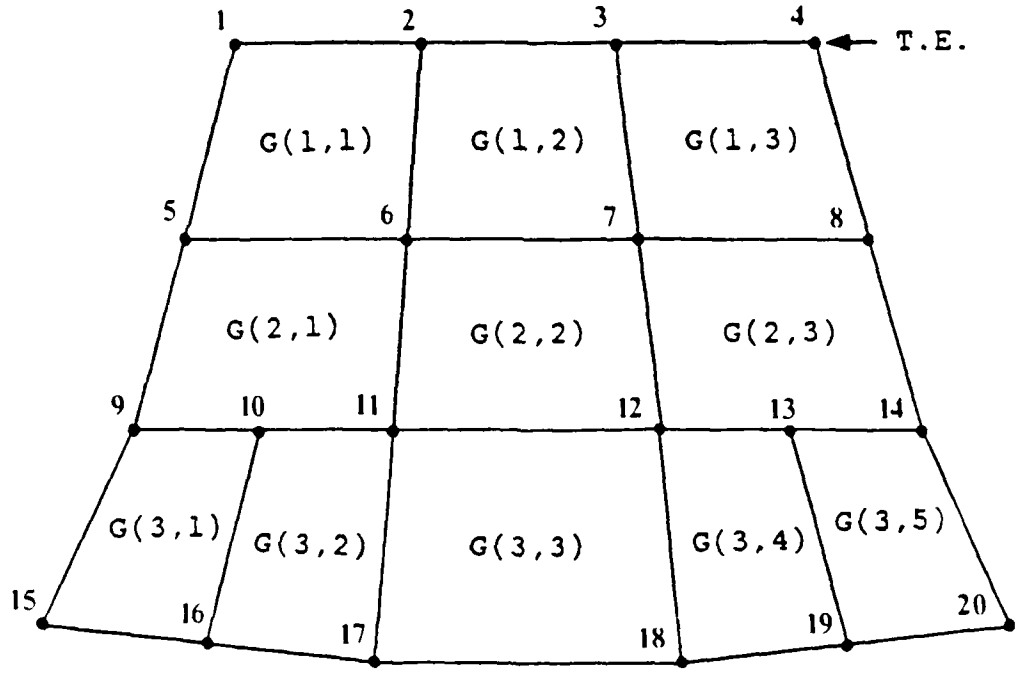

Figure 13. Three-Dimensional Wake Formation

Chapter IV

Results

Two geometries were investigated for the analysis. In both cases a unit area aspect ratio delta wing was modeled using 30 rows of elements. The wing was analyzed at 20.5 and 30 degrees angle of attack. It is known that vortex breakdown does not occur over a delta wing with an aspect ratio of one at 20.5 degrees angle of attack. Therefore, this was calculated as a baseline. An angle of attack of 30 degrees was used to determine if paneling methods can compute the vortex bursting that occurs over the delta wing. In order to establish if vortex bursting occurs, the criteria established by O'Neil, Barnett, and Louie shall be used. In both cases, the fluid was impulsively started. The Kutta weighting values for the 20.5 and 30 degree angle of attacks were 0.50 and 0.515 respectively. These values were sufficient to sustain the wake tangency condition with the surface of the airfoil throughout the calculations. Figure 14 presents the element composition of the delta wing.

Both calculations were carried out to produce one chord length of wake. The time step was set equal to the height of the triangular elements. This produced wake elements

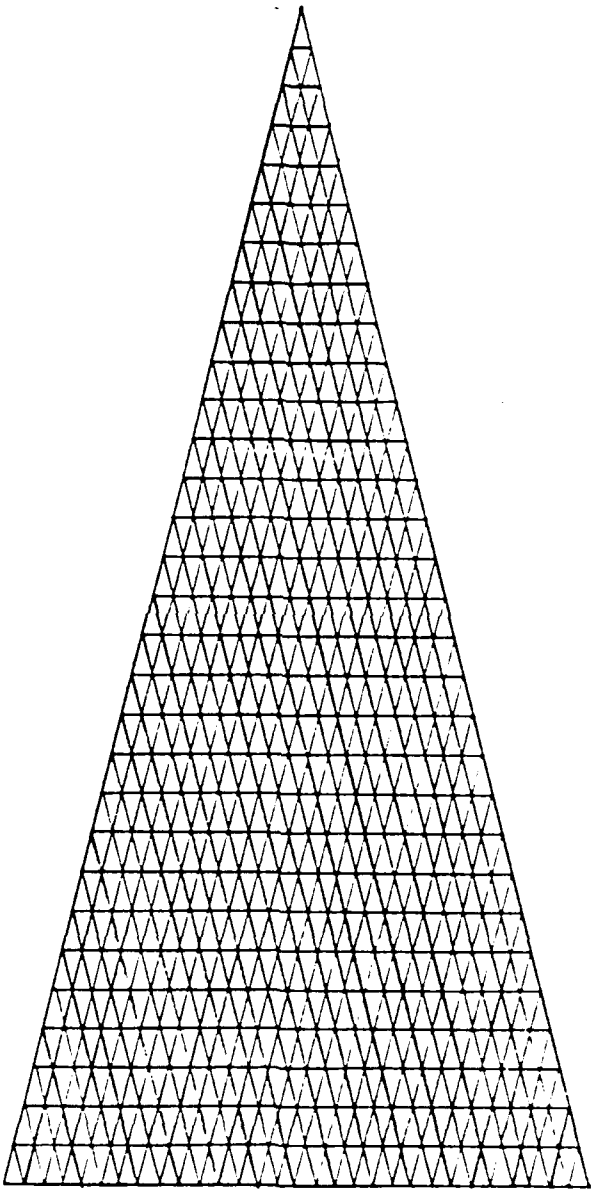

Figure 14. Element Composition of a Unit Area Aspect Ratio Delta Wing

that were initially geometrically square and required 30 time steps to produce one chord length of wake. Figures 15, and 16 show the wake mesh at this time for the 20.5, and 30 degrees angle of attack. The view was from above the airfoil. In both figures the wing elements were not presented to help clarify the pictures. The 'X' represents the body frame origin, and the front apex of the wing. The trailing edge is easily recognized as the vertical line where the wake is orginating. The paneling method computes both the leading edge and the trailing edge vortices typical of the flow over delta wings. However, the method breaks down for the 30 degree angle of attack where these two vortices meet and combine. This was due to the first order convection scheme used for the wake nodes, convecting the cores at the local particl velocity. As two vortex cores come within close proximity of each other, their respective velocities increase dramatically. This is evident from equation 2-29. Figures 17, and 18, provide a hidden line picture that provides a clear view of the leading edge vortices and the destruction of the wake mesh for the 30 degree angle of attack. For the 20 degree angle of attack, the leading edge vortex expands in a continuous manner as it is convected downstream. However, viewing the leading edge vortex for the 30 degree angle of attack, shows a perturbation and enlargement of the vortex approximately at the two-thirds

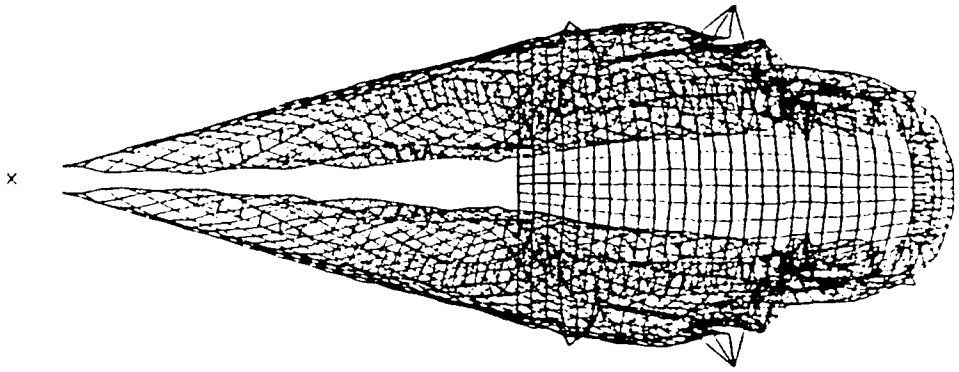

Figure 15. Wake Mesh at 20.5 Degrees Angle of Attack and 30 Time Steps

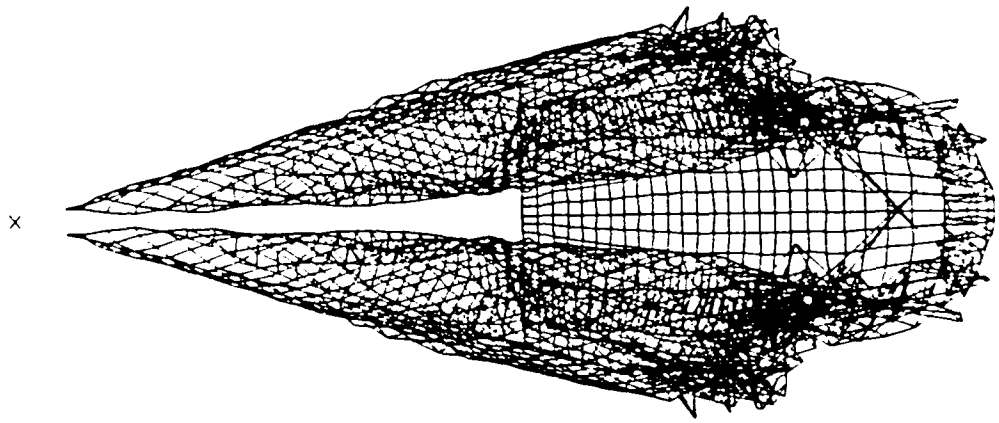

Figure 16. Wake Mesh at 30 Degrees Angle of Attack and 30 Time Steps

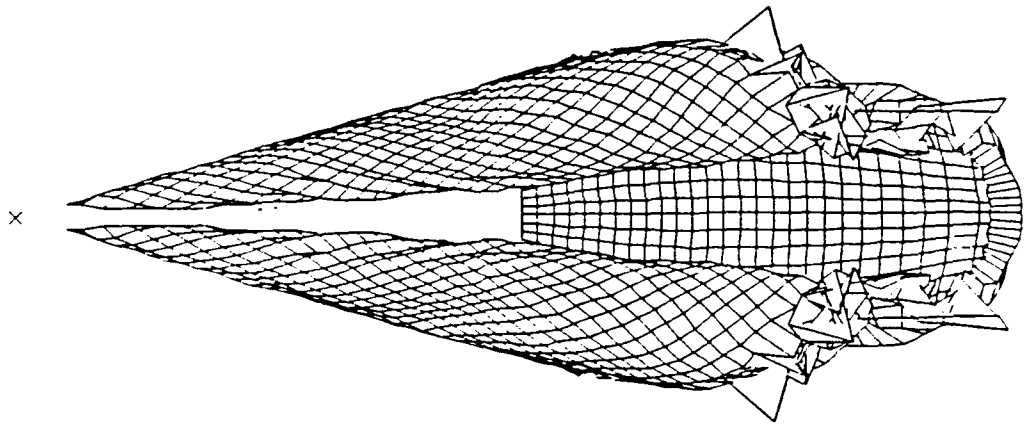

Figure 17. Hidden Line View of the Wake Mesh at 20.5 Degrees Angle of Attack

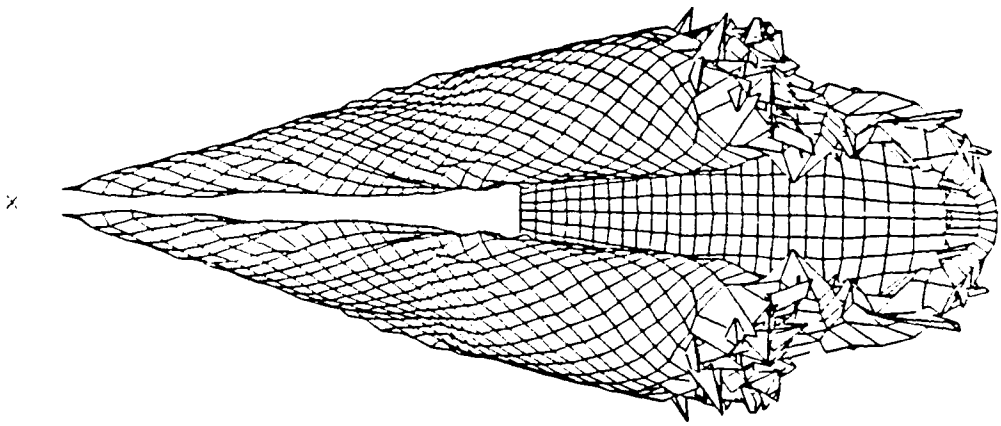

Figure 18. Hidden Line View of the Wake Mesh at 30 Degrees Angle of Attack

cord position. This fits the description of vortex-breakdown provided by O'Neil, Barnett, and Louie. Cross-sections of the leading-edge vortices are taken in the Y-Z plane just along the trailing edge of the wing, Figures 19, and 20. Here the paneling method performed well by modeling the vortex roll-up. The vortex for the 30 degree angle of attack is larger than the vortex produced at an angle of attack of 20 degrees, as would be expected. Further investigation into the pressure gradients in the spanwise direction should be performed to verify this result.

Figures 21, and 22, show the coefficient of pressure distribution in the spanwise directions for 20.5 and 30 degrees angle of attack respectively. The length in the spanwise direction is normalized by one-half the local span (Y_{max}). The pressure distributions are provided at one-half, two-thirds, and five-sixths chords and at the trailing edge. These curves are typical of the trends investigated experimentally under similar conditions over delta wings. It is evident here that the Kutta condition is not satisfied at the leading edges as the coefficient of pressure does not equal zero at the end of each curve, as it should. The rise in the curves are the enhanced lift provided by the suction induced by the leading edge vortices. A peculiar decrease in the coefficient of pressure, or decrease in lift, is conspicuous at the two-thirds chords position at 30 degrees

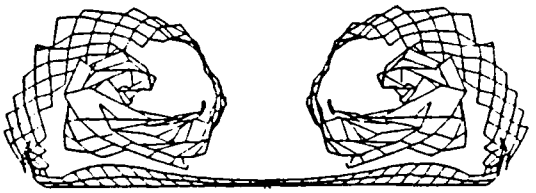

Figure 19. Trailing Edge Cross Section of the Wake for 20.5 Degrees Angle of Attack

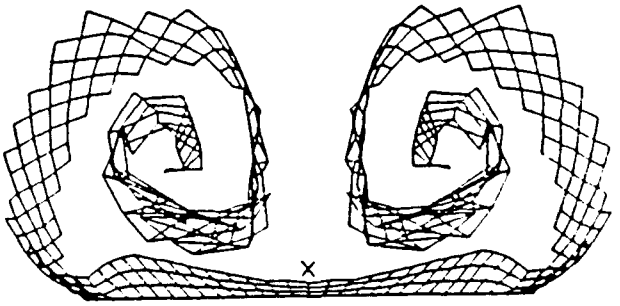

Figure 20. Trailing Edge Cross Section of the Wake for 30 Degrees Angle of Attack

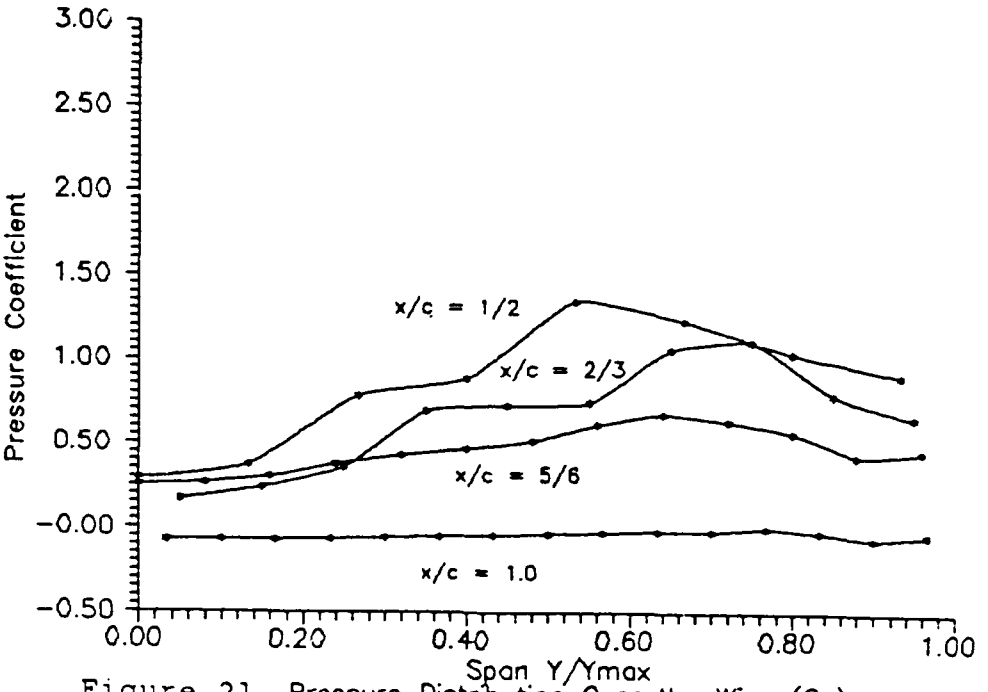

Figure 21. Pressure Distribution Over the Wing (Cp)
Angle of Attack = 20.5 degrees
One Chord Length of Wake

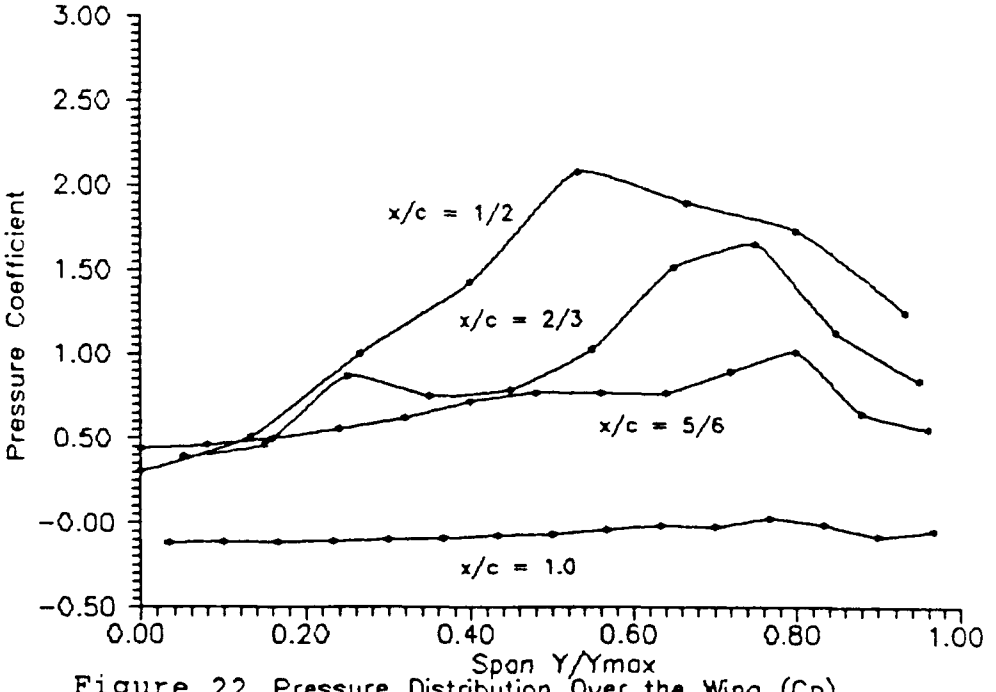

Figure 22. Pressure Distribution Over the Wing (Cp)
Angle of Attack = 30 degrees
One Chord Length of Wake

angle of attack. This corresponds to the chordwise location of the vortex perturbation. These sharp gradients in the pressure coefficient, however, contradict the vortex breakdown criteria as stated previously.

In an attempt to eliminate the sharp pressure gradients, the calculations were continued for another ten time steps, or one-third chord length. This was performed to allow the wake to split more thoroughly, and hence, create the mild pressure gradients required to meet the vortex breakdown criteria. Figures 23, and 24, show the wake mesh, at this time, for the 20.5 and 30 degrees angle of attack respectively. At this time the wake is beginning to deteriorate for the 20.5 degrees angle of attack. The wake has severely degenerated for the 30 degree angle of attack behind the wing, although, it still retains its structure over the wing. The perturbation in the leading-edge vortex is still evident and implies the existence of vortex breakdown.

Again the pressure distributions in the spanwise direction, at the same chordwise positions, over the wing are reviewed. The coefficient of pressure distributions are provided in Figures 25, and 26. Each position along the surface of wing at 20.5 degrees angle of attack provides

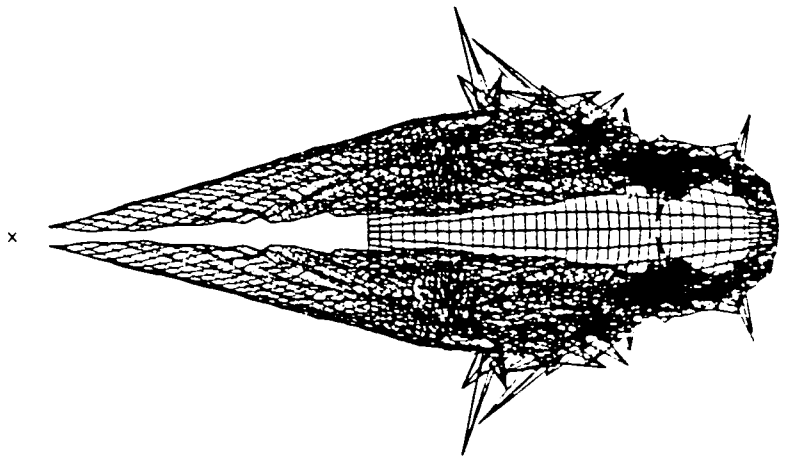

Figure 23. Wake Mesh at 20.5 Degrees Angle of Attack and 40 Time Steps

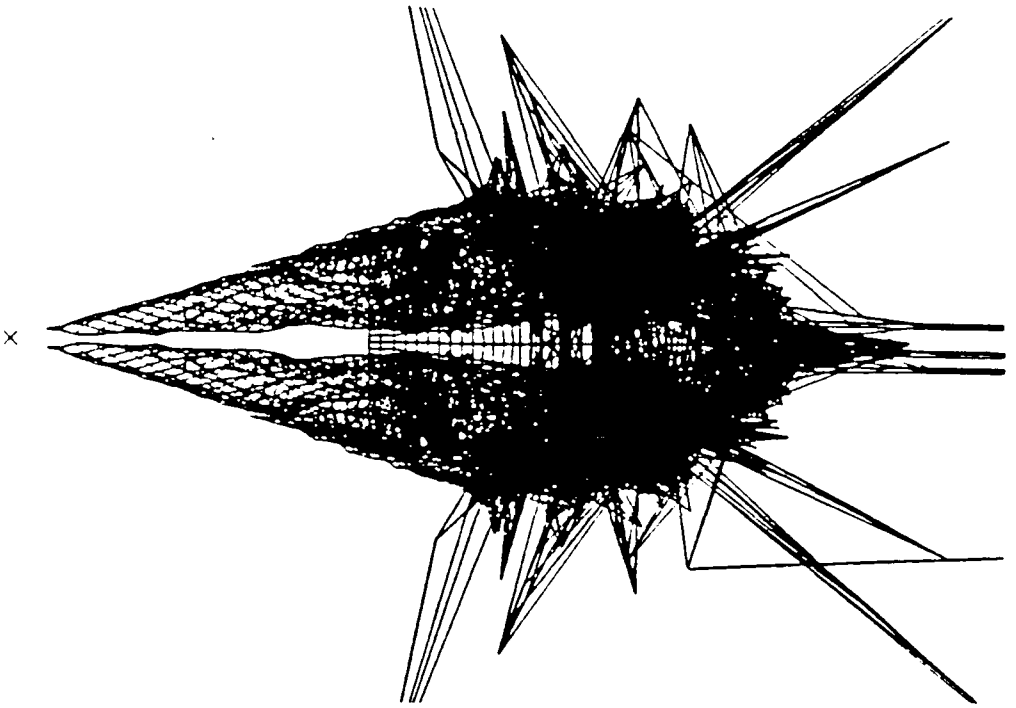

Figure 24. Wake Mesh at 30 Degrees Angle of Attack and 40 Time Steps

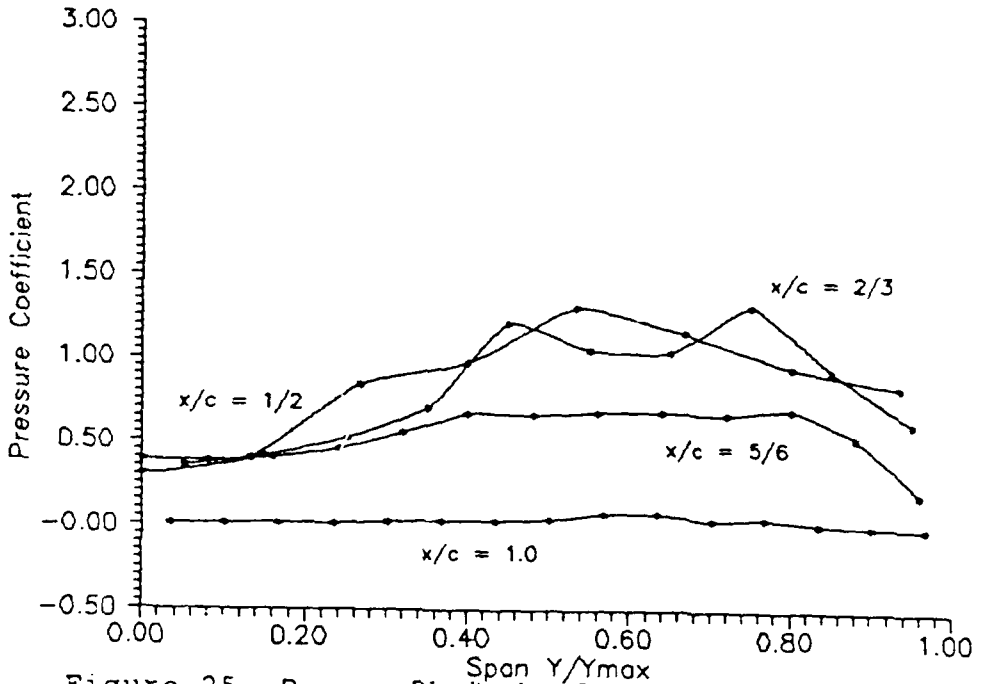

Figure 25. Pressure Distribution Over the Wing
Angle of Attack = 20.5 Degrees
1 1/3 Chords Length of Wake

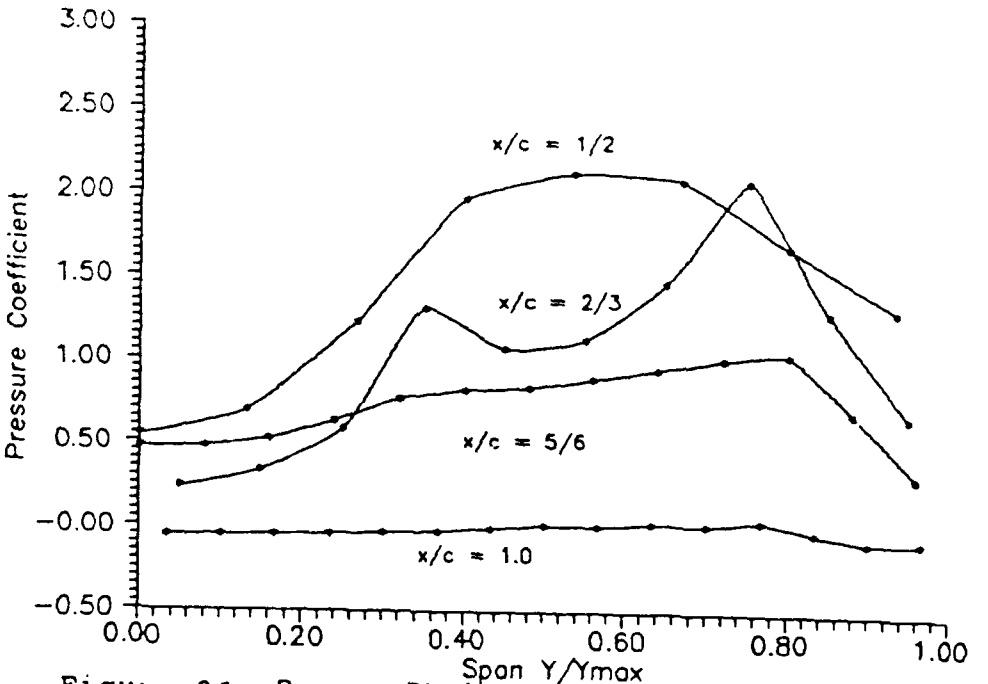

Figure 26. Pressure Distribution Over the Wing
Angle of Attack = 30 Degrees
1 1/3 Chords Length of Wake

more lift with the increased wake. The pressure gradient at the two-thirds chord position, at an angle of attack of 30 degrees, has not diminished, and has actually increased with the increased amount of wake. However, this is the only position that exhibits a decrease in the amount of lift provided for both calculations. This severe pressure gradient again fails the criteria for vortex bursting over the wing.

Due to the extreme wake degeneration for the 30 degrees angle of attack, a question arises if this was a valid calculation. In an attempt to answer this query, another calculation was performed for the 30 row delta wing at an angle of attack of 30 degrees. However, for this computation the wake was not allowed to split beyond the one and one-third chords position from the leading apex of the wing. The wake mesh is provided in Figure 27. For this calculation the wake has not deteriorated to the point of the previous computation. However, the coefficient of pressure distribution over the wing is equivalent to the preceding coefficient of pressure distribution, Figure 28. This provides the unexpected result that the pressure distribution over the wing is relatively independent to the wake downstream.

A comparision of the wake cross sections at two-thirds, and five-sixths chords length and at the trailing edges are provided for the 30 and 20.5 degrees angle of attack computations in Figures 29, 30, and 31, respectively. The

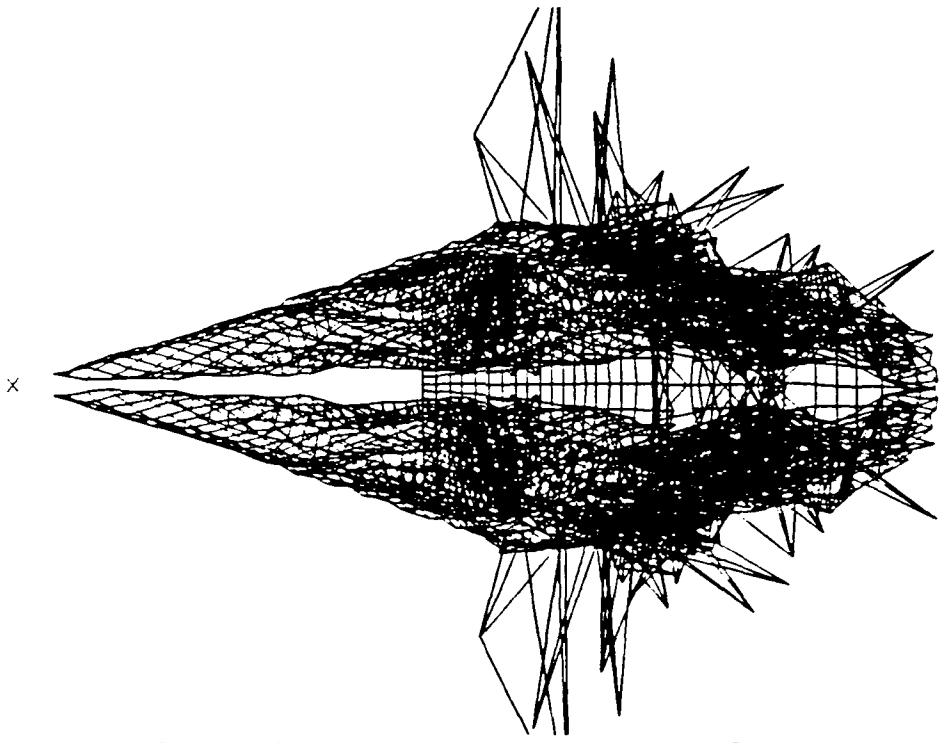

Figure 27. Wake Mesh at 30 Degrees Angle of Attack and 40 Time Steps, No Splitting Beyond -40

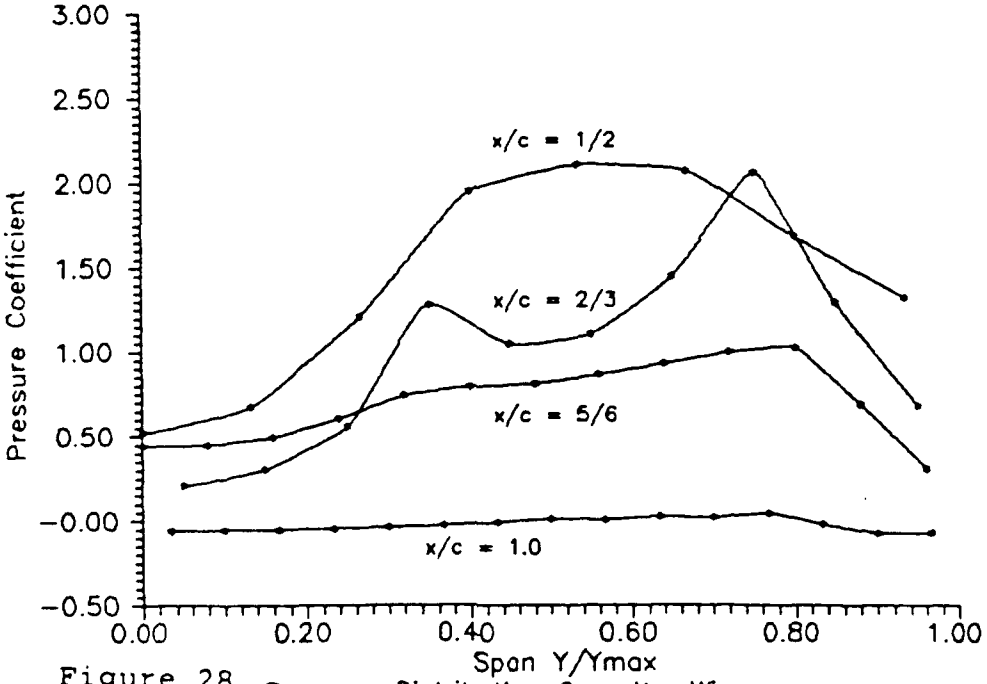

Figure 28. Pressure Distribution Over the Wing
Angle of Attack = 30 Degrees, No Splitting Beyond -40
1 1/3 Chords Length of Wake

comparisons are performed at 40 time steps. At the two-thirds chord position, the wake has only progressed one complete revolution. At the trailing edge, it has developed to approximately one and one-half revolutions. At every chordwise postion, the wakes generated by the two calculations are analogous. The prominent distinction between the different angle of attacks is the magnitude of the leading edge vortex. Again this leads to the conclusion that vortex breakdown does not exist in the 30 degrees angle of attack calculation.

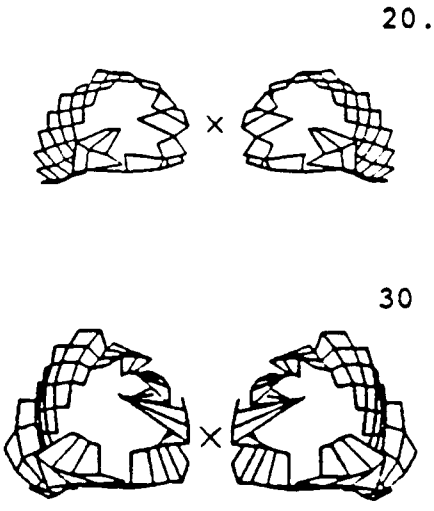

Figure 29. Vortex Comparisons At the Two-Thirds Chordwise Position

20.5 Degrees

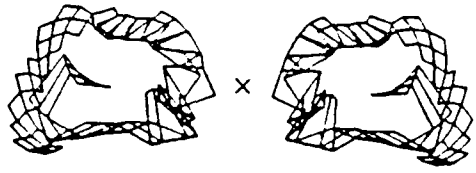

30 Degrees

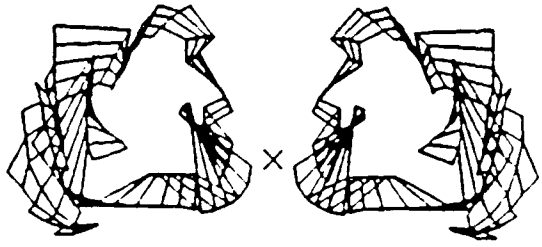

Figure 30. Vortex Comparisons At the Five-Sixths Chordwise Position

20.5 Degrees

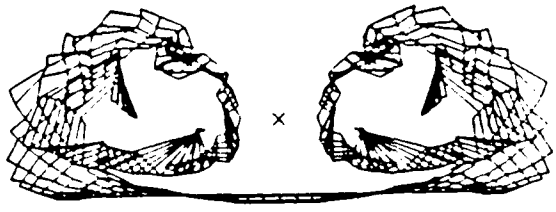

30 Degrees

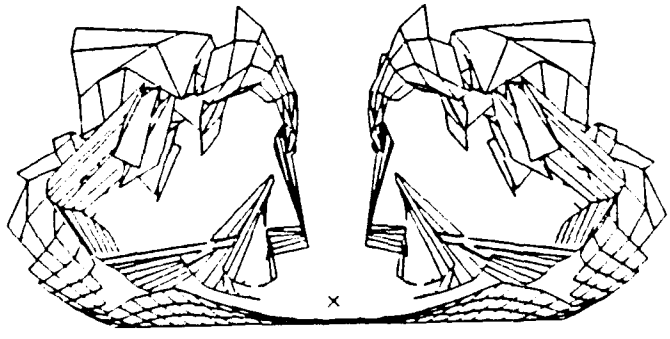

Figure 31. Vortex Comparisons At the Trailing Edge

Chapter V

Conclusions and Recommendations

A unit aspect ratio delta wing was analyzed to determine if a unsteady vortex panel method could compute the bursting of the leading edge vortex. The criteria for which vortex bursting would be identified was that defined by O'Neil, Barnett, and Louie; a degeneration of the leading-edge vortex combined with relatively mild gradients. (6:220) A two-dimensional vortex panel method was employed to evaluate wake splitting procedures of the vortex cores representing the vortex sheet, or wake. The worthier splitting scheme was then extended to the three-dimensional panel methods. The weighting values applied to the Kutta equations along the leading edges were determined to be problem dependent. No relationship between the airfoil parameters and the weighting value could be determined. A finite element technique was employed to manage the wake data. This provided a reduction in the amount of computer time and memory required for a given calculation. A unit area aspect ratio delta wing analysis was performed. A qualitative comparison between 20.5 and 30 degrees angle of attack was accomplished. At the 30 degrees angle of attack the paneling method produced a perturbation and enlargement in the

leading edge vortex at the two-thirds chordwise position. However, wake cross-sections and coefficient of pressure comparisons to the 20.5 degrees angle of attack computation determined that the panel methods did not calculate vortex breakdown.

A possible explanation of the failure to predict vortex bursting was the splitting method employed. The process would check the spanwise distance of the wake elements, and split the elements in the spanwise direction if warranted. This was based on the premise that the wake is continuously diverging. However, the wake elements would also elongate in the chordwise direction. This is apparent in Figures 29 through 31. The area most susceptible to this stretching is in the leading edge vortex. A method of splitting the wake in the chordwise direction should be performed before further analysis of vortex breakdown is accomplished.

The vortex sheet generated off the edges of the airfoil, in this effort, was used as the flow visualization of the wake. Further analysis could be performed by the inclusion of Lagragian points within the flow field. This could easily be incorporated within the computer code and would possibly provide further insight into the problem.

Another area of interest would be the implementation of a second order convection scheme of the wake nodes. The intermingling of the leading edge and trailing edge vorti-

cies induced unrealistically high velocities of the wake nodes. Thus, the deterioration of the wake mesh. A second order convection scheme could possibly eliminate this deficiency. However, the use of a higher-order method would require more computer time, but should still be performed to determine its benefits.

Bibliography

1. Abbott, Ira H. and Von Doenhoff, Albert E. Theory of Wing Sections, New York, NY: Dover Pulblications, Inc. 1959.

2. Ekaterinaris, J. A. and Schiff, L. B. "Vortical Flows over Delta Wings and Numerical Prediction of Vortex Breakdown," AIAA 28th Aerospace Sciences Meeting, 90-0102, 1-22 (January 1990).

3. Hitzel, Stephan M. "Wing Vortex-Flows Up Into Vortex-Breakdown - A Numerical Simulation," AIAA 6th Applied Aerodynamics Conference, 88-2518-CP, 73-83 (June 1988).

4. Karamcheti, Krishnamurty. Principals of Ideal-Fluid Aerodynamics, Malabar, FL: Robert E. Krieger Publishing Co., Inc. 1966.

5. Mook, D. T. and others. "On the Numerical Simulation of the Unsteady Wake Behind an Airfoil," AIAA 25th Aerospace Sciences Meeting, 87-0190, (1987).

6. Mracek, Capt. Curtis Paul. Unsteady Potential-Flow Solution Using Vortex Panels Coupled With Dynamics and Controls. PHD dissertation. Virginia Polytechnic Institute and State University, Blacksburg, VA, July 1988.

7. O'Neil, P. J. and others. "Numerical Simulation of Leading-Edge Vortex Breakdown Using an Euler Code," AIAA 7th Applied Aerodynamics Conference, 89-2189-CP, 218-226, (July-August 1989).

VITA

Don Lorey was born on Jan 24, 1962, in Escanaba, Michigan. After moving to the lower peninsula he graduated from Linden High School, Linden Michigan. He then entered Michigan State University, graduating with at Bachelor of Science degree in Mechanical Engineering in 1984. Immediately thereafter, accepted a Commission in the United States Air Force, and three months later entered active duty. His first assignment was at the Air Force Armament Laboratory, Eglin AFB, FL, where he had the distinct pleasure of applying his education in the use of finite element and finite difference techniques in the development of new and unique warheads. In 1985 he met his wife to be, Lora Coleman. Nine months later they were married on May 25, 1986. In the summer of 1989 he entered the Air Force Institute of Technology in pursuit of a Master of Science degree.

REPORT DOCUMENTATION PAGE

Form Approved
OMB No. 0704-0188

1 AGENCY USE ONLY (Leave blank)	2 REPORT DATE	3 REPORT TYPE AND DATES COVERED
	December 1990	

4 TITLE AND SUBTITLE

VORTEX BURSTING OVER A UNIT ASPECT RATIO DELTA WING USING VORTEX-PANEL METHODS

5 FUNDING NUMBERS

6 AUTHOR(S)

Donald A. Lorey, Captain, USAF

7 PERFORMING ORGANIZATION NAME(S) AND ADDRESS(ES)

Air Force Institute of Technology,
WPAFB OH 45433-6583

8 PERFORMING ORGANIZATION REPORT NUMBER

AFIT/GAE/ENA/90D-14

9 SPONSORING/MONITORING AGENCY NAME(S) AND ADDRESS(ES)

10 SPONSORING/MONITORING AGENCY REPORT NUMBER

11 SUPPLEMENTARY NOTES

12a DISTRIBUTION/AVAILABILITY STATEMENT

Approved for public release:
distribution unlimited

12b DISTRIBUTION CODE

A unit aspect ratio delta wing is analyzed to determine if a unsteady vortex panel method can calculate the vortex bursting of the vortex developed along the leading-edge. A two-dimensional vortex panel method is used to investigate wake splitting schemes of the vortex cores that comprise the vortex sheet, or wake. The worthier of the splitting methods is later implemented into the three-dimensional wake. The weighting values of the Kutta equations are investigated for the leading-edges, and are determined to be problem specific. An alternative approach to the management of the wake data is presented and implemented. The delta wing is then analyzed for 20.5 and 30 degrees angle of attack. The panel method produced a perturbation and enlargement in the wake at the two-thirds chord position over the wing at 30 degrees angle of attack, indicative of vortex breakdown. However, a qualitative comparison with the results of the 20.5 degree angle of attack calculation negates this conclusion. Vortex bursting was not evident over the wing at 30 degrees angle of attack.

14 SUBJECT TERMS

Vortex Bursting, Vortex Breakdown,
Vortex Panel Methods, Vortex Lattice Methods

15 NUMBER OF PAGES

66

16 PRICE CODE

17 SECURITY CLASSIFICATION OF REPORT	18 SECURITY CLASSIFICATION OF THIS PAGE	19 SECURITY CLASSIFICATION OF ABSTRACT	20 LIMITATION OF ABSTRACT
Unclassified	Unclassified	Unclassified	UL